APRIL 26, 2018
VOLUME 122
NUMBER 16
pubs.acs.org/JPCC

# THE JOURNAL OF PHYSICAL CHEMISTRY C

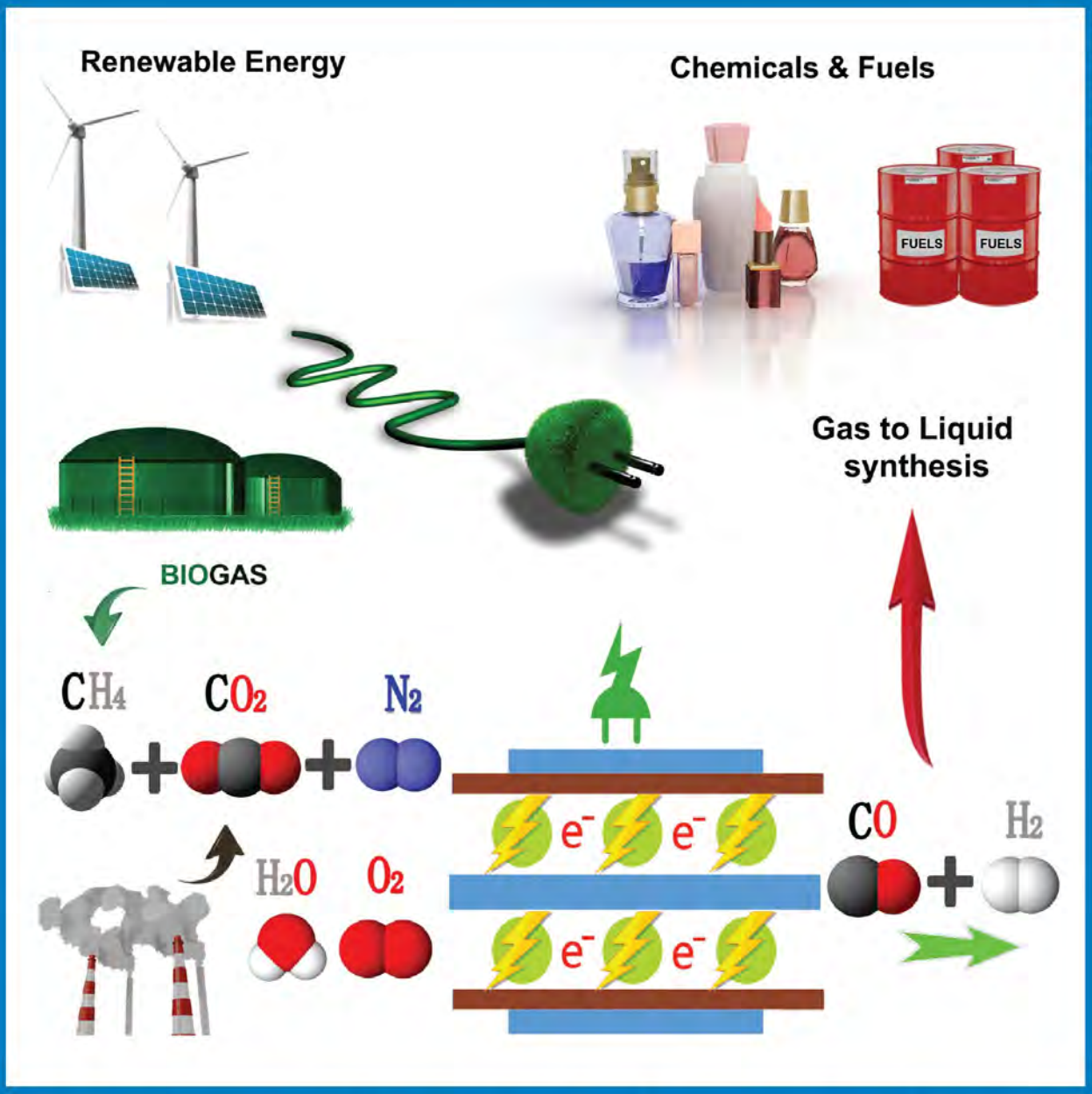


Plasma-based $CO_2$ Conversion and $CH_4$ Reforming in Combination with $O_2$, $H_2O$, and $N_2$

ENERGY CONVERSION AND STORAGE, OPTICAL AND ELECTRONIC DEVICES, INTERFACES, NANOMATERIALS, AND HARD MATTER

ACS Publications
Most Trusted. Most Cited. Most Read.
www.acs.org

THE JOURNAL OF PHYSICAL CHEMISTRY C

Feature Article

Cite This: J. Phys. Chem. C 2018, 122, 8704−8723

pubs.acs.org/JPCC

# Modeling Plasma-based $CO_2$ and $CH_4$ Conversion in Mixtures with $N_2$, $O_2$, and $H_2O$: The Bigger Plasma Chemistry Picture

Weizong Wang,*[,†,∥] Ramses Snoeckx,*[,†,‡,∥] Xuming Zhang,[‡,§] Min Suk Cha,[‡] and Annemie Bogaerts*[,†]

[†]Research Group PLASMANT, Department of Chemistry, University of Antwerp, Universiteitsplein 1, B-2610 Wilrijk-Antwerp, Belgium

[‡]King Abdullah University of Science and Technology (KAUST), Clean Combustion Research Center (CCRC), Thuwal 23955, Saudi Arabia

[§]College of Environmental Science and Engineering, Zhejiang Gongshang University, Xiasha High Education District, Hangzhou, Zhejiang Province, China

Supporting Information

**ABSTRACT:** Because of the unique properties of plasma technology, its use in gas conversion applications is gaining significant interest around the globe. Plasma-based $CO_2$ and $CH_4$ conversion has become a major research area. Many investigations have already been performed regarding the single-component gases, that is, $CO_2$ splitting and $CH_4$ reforming, as well as for two-component mixtures, that is, dry reforming of methane ($CO_2/CH_4$), partial oxidation of methane ($CH_4/O_2$), artificial photosynthesis ($CO_2/H_2O$), $CO_2$ hydrogenation ($CO_2/H_2$), and even first steps toward the influence of $N_2$ impurities have been taken, that is, $CO_2/N_2$ and $CH_4/N_2$. In this Feature Article we briefly discuss the advances made in literature for these different steps from a plasma chemistry modeling point of view. Subsequently, we present a comprehensive plasma chemistry set, combining the knowledge gathered in this field so far and supported with extensive experimental data. This set can be used for chemical kinetics plasma modeling for all possible combinations of $CO_2$, $CH_4$, $N_2$, $O_2$, and $H_2O$ to investigate the bigger picture of the underlying plasmachemical pathways for these mixtures in a dielectric barrier discharge plasma. This is extremely valuable for the optimization of existing plasma-based $CO_2$ conversion and $CH_4$ reforming processes as well as for investigating the influence of $N_2$, $O_2$, and $H_2O$ on these processes and even to support plasma-based multireforming processes.

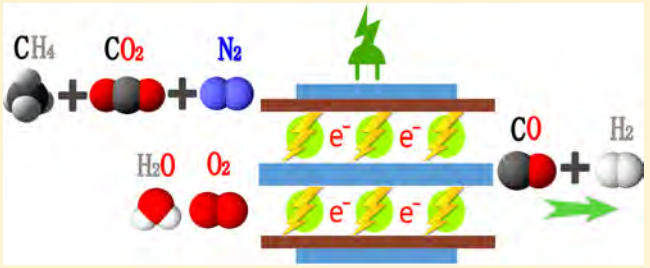


## 1. INTRODUCTION: PLASMA TECHNOLOGY

Today, more than ever, plasma technology lies at the base of modern technology, as the entire microelectronics industry relies on plasma−surface interactions.[1,2] These interactions make it possible for scientists to extend Moore's law by providing the current nanometer resolution of microprocessors.

In general, plasma consists of various types of ions (both positive and negative), electrons, and a large variety of neutral species, that is, different types of atoms, molecules, radicals, and excited species. This makes plasma a highly reactive, but complex, —chemical cocktail, which is of interest to many potential applications.[1,3,4]

Plasma is often referred to as the "fourth state of matter". Indeed, upon increasing energy input, matter transforms in the sequence: solid, liquid, (neutral) gas, and finally ionized gas or plasma. Although plasma might not be so widely known as the other three states of matter, 99% of the visible universe is actually in plasma state, mainly as stars (including our Sun) and interstellar matter. Furthermore, natural plasmas also occur on Earth in the form of most natural occurring weather phenomena that emit light, for example, lightning, auroras (Borealis and Australis), Saint Elmo's fire, and red sprites.

Beside natural plasmas, two main groups of man-made plasmas are distinguished, that is, high-temperature or fusion plasmas and low-temperature plasmas or gas discharges. The latter group can be further subdivided based on whether the plasma is in thermal equilibrium. Because of the multitude of different types of species, which can all have different temperatures and degrees of freedom, plasma can exhibit, and is defined by, multiple temperatures, for example, gas temperature, electron temperature, ion temperature, vibrational temperature, and rotational temperature. When in a localized area, these temperatures are the same, and the plasma is said to be in "local thermodynamic equilibrium" (LTE) and mostly called a "thermal plasma". In the other case, the plasma is said to be in "nonlocal thermodynamic equilibrium" (non-LTE), and mostly called a "nonthermal plasma".

One of the main reasons why low-temperature (non-LTE) plasmas have such a large potential for a wide variety of applications is their capability of producing a reactive chemical

Received: October 26, 2017
Revised: January 1, 2018
Published: January 18, 2018





DOI: 10.1021/acs.jpcc.7b10619
J. Phys. Chem. C 2018, 122, 8704−8723

environment while staying at room temperature. This is possible due to most of the energy being directed into the electrons, leading to a much higher electron temperature ($T_e$) compared with the gas temperature ($T_g$). Subsequently, these highly energetic electrons can activate the gas and initiate reactions by electron impact collisions rather than the classical form of energy used in industry, that is, heat.

Applications range from materials science (e.g., coating deposition, surface modification, nanotechnology, and chip manufacturing, as mentioned above) over lighting, lasers, and plasma displays (as plasma emits light due to the presence of many excited species), to analytical chemistry, thrusters, as well as environmental, energy, and medical applications (e.g., sterilization, wound healing, and even cancer treatment).[1,3,4] Environmental and energy applications include, among others, air pollution control,[5] nitrogen fixation from the air to form ammonia and nitric oxides,[6,7] hydrocarbon reforming,[8−10] and $CO_2$ conversion into value-added chemicals and fuels.[11] These applications often use a combination of plasma with catalysts, yielding plasma catalysis.[11−14]

To improve these applications, a good knowledge of the underlying plasma processes is indispensable. The latter can be obtained by experiments and computer modeling. Because detailed measurements inside the plasma are not always straightforward, modeling can indeed be of great value. This Feature Article will focus on the continuous research efforts in modeling the plasma chemistry for the growing application of low-temperature (non-LTE) plasmas used for $CO_2$ conversion and $CH_4$ reforming as well as combinations with other gases and highlight the contributions of the PLASMANT research group in this field.[15,16] On the basis of the gained knowledge so far and an extensive set of experiments carried out for various gas mixtures and mixing ratios, a new comprehensive plasma chemistry model is presented that can be used to describe the underlying mechanisms of $CO_2$ and $CH_4$ conversion, also in the presence of $N_2$, $O_2$, and $H_2O$.

## 2. PLASMA CHEMISTRY MODELING FOR $CO_2$ CONVERSION AND $CH_4$ REFORMING

Interest in the application of plasma technology for $CO_2$ conversion and $CH_4$ reforming has been growing rapidly.[9,11,17−20] Because of the adverse effects of climate change on our society, the conversion of these gases into value-added chemicals and fuels is considered as one of the great challenges of the 21st century.[21] Successfully converting the greenhouse gas $CO_2$ would be interesting from both an economic and ecological perspective. This would lead to the successful generation of an artificial closed carbon loop, which fits into the "cradle-to-cradle" concept,[22] that is, upcycling waste material into new feedstock. Additionally, with the increase in biogas, landfill gas, and hydrogenation of $CO_2$ to $CH_4$, the straightforward reforming of $CH_4$ into liquid products would be beneficial because the energy density of liquid fuel is much higher and it is easier to transport.[23,24]

As outlined in an extensive recent review on the use of plasma technology for $CO_2$ conversion,[11] "Plasmas possess some important advantages over other (novel) technologies for the conversion of $CO_2$ and $CH_4$: (i) they can operate at room temperature using any source of (renewable) electricity, (ii) they have a large flexibility in terms of the feeds that need to be processed, (iii) they provide an extremely flexible "turnkey" process, which allows for the efficient storage of energy, peak shaving and grid stabilization, (iv) the reactors have low investment and operating costs, (v) they have a simple scalability both in size and applicability, and (vi) last but not least, the technology does not rely on rare earth materials—making it rather unique at this point. This unprecedented combination of features gives plasmachemical conversion a very high overall flexibility, making it an extremely useful and valuable technology for CCU."

To improve this application, several research groups developed models for chemical kinetics simulations to better understand the underlying mechanisms, and a brief literature overview will be given below. This development can be subdivided into three main stages: (1) modeling single-component molecular gases, that is, plasma-based $CO_2$ splitting and $CH_4$ reforming; (2) investigating common two-component mixtures, that is, dry reforming of methane ($CO_2/CH_4$), partial oxidation of methane ($CH_4/O_2$), artificial photosynthesis ($CO_2/H_2O$), and $CO_2$ hydrogenation ($CO_2/H_2$); and (3) moving toward more realistic gas mixtures by investigating the effect of $N_2$ both as admixture and impurity, that is, $CO_2/N_2$ and $CH_4/N_2$. The following subsections will be divided according to these three stages.

The knowledge obtained during these different stages is now combined into one comprehensive chemical kinetics plasma model for use in low-temperature (non-LTE) plasmas, presented for the first time in this Feature Article. Therefore, in the following subsections, we will each time compare the $CO_2$ or $CH_4$ conversion, calculated with this new model, with our previous (published) experimental data to step-by-step validate the individual chemistry sets. This validation will be performed for a dielectric barrier discharge (DBD) plasma, as the chemistry model presented in this Feature Article is specifically developed for this type of plasma. A DBD plasma is created by applying a potential difference between two electrodes, of which at least one is covered by a dielectric barrier. For $CO_2$ and $CH_4$ conversion applications, a tubular DBD reactor is most often used,[11] consisting of an inner electrode surrounded by a dielectric tube, covered by an outer electrode (see Figure 1).

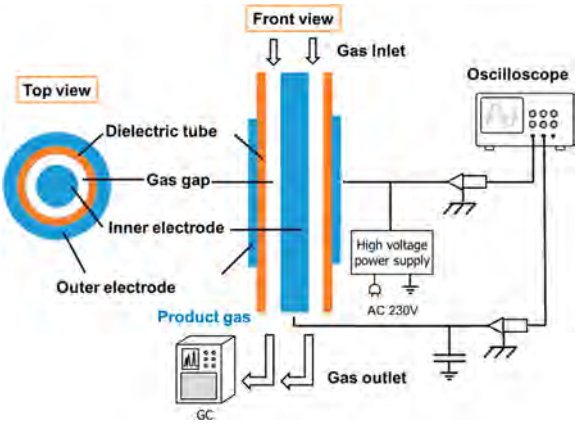


**Figure 1.** Schematic diagram of a dielectric barrier discharge (DBD).

Subsequently, in Section 3 we will present this new comprehensive chemical kinetics plasma model for use in low-temperature (non-LTE) plasmas. The applications of this extensive model are broad. They can range from very specific investigations, like the effect of $CH_4$ on $NO_x$ mitigation for $CO_2/N_2$ plasmas, to realistic industrial gas mixtures for dry reforming of methane by inclusion of $N_2$, as well as unravelling the possibilities for plasma-based multireforming processes. Furthermore, this chemistry set can also be used as a foundation to build a comprehensive computational data set in the field of plasma-assisted combustion.[25,26] Finally, certain data from this set could even be used for exotic models, like planetary atmosphere and spacecraft re-entry modeling.[27,28]



DOI: 10.1021/acs.jpcc.7b10619
J. Phys. Chem. C 2018, 122, 8704−8723

**2.1. Single-Component Molecular Gases.** With the breakthrough of sufficient, and continuously increasing, computational power available to researchers, plasmachemical modeling efforts could expand from simple noble gases toward reactive molecular gases.

In the past 10 years many different plasmachemical kinetic models have been developed for pure $CO_2$ splitting in various kinds of plasmas.[9,29−49] Several of these models have been developed in the research group PLASMANT.[29−39] Furthermore, there is also interest in pure $CH_4$ reforming, also known as "the pyrolysis of methane", used to synthesize higher hydrocarbons.[9] Few models exist in literature,[50−53] of which one has been developed in the research group PLASMANT.[52]

Figure 2 illustrates a comparison of the calculated $CO_2$ conversion using our new comprehensive model (see Section 3) with

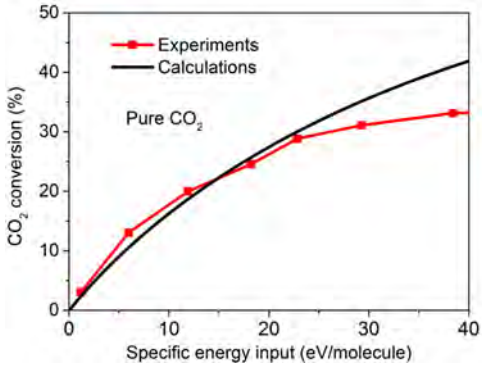


**Figure 2.** Comparison of the calculated $CO_2$ conversion, as obtained from our new comprehensive plasma chemistry model, with measured data adopted from ref 29, as a function of SEI at a fixed plasma power of 40 W and varying gas flow rate.

measured values for a pure $CO_2$ DBD plasma[29] at a fixed plasma power of 40 W and varying the gas flow rate to yield different values of the specific energy input (SEI). The $CO_2$ conversion is mainly caused by electron impact dissociation under these conditions (see below and ref 29). The conversion gradually increases with rising SEI, in both the experiments and calculation results, which is logical because more energy is put into the system. Above 25 eV/molecule, the model does not yet show saturation, although it is observed in the experimental data. However, as described in the review of Snoeckx and Bogaerts,[11] these higher SEI values are not attractive because of very low energy efficiency. The recommended SEI range is on the order of 0.1 to 5 eV/molecule. Therefore, we may conclude that the agreement between model and experiments is good, especially in the SEI region of most practical interest.

**2.2. Two-Component Mixtures.** With even more computing power and the successful development of models for simulating single-component molecular gases, as described above, the combination of these models into two-component reactive mixtures was the logical, albeit not always easy, next step.

*2.2.1. Dry Reforming and Partial Oxidation of Methane.* The combined conversion of $CO_2$ and $CH_4$, also known as "dry reforming of methane" (DRM), has been extensively studied,[9,11] and a variety of models have been developed in literature.[54−66] Again, several of these models have been developed within the research group PLASMANT.[63−66] Besides $CO_2$, another stronger oxidant used to reform $CH_4$ is $O_2$, and this combination is known as "partial oxidation of methane" (POX).[9] Several modeling investigations exist in literature,[66−72] including one from our group PLASMANT.[66] Although this process leads to higher $CH_4$ conversions than DRM, its strong oxidative character causes a total oxidation of $CH_4$, producing $CO_2$, and is therefore of less interest.

Figure 3 illustrates the calculated absolute conversions of $CH_4$ and $CO_2$ in plasma-based DRM as a function of discharge power

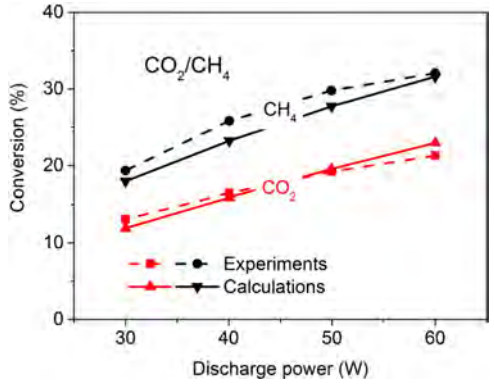


**Figure 3.** Comparison of the calculated absolute conversion of $CO_2$ and $CH_4$, as obtained from our new comprehensive plasma chemistry model, with measured data adopted from ref 63 in a 1:1 $CO_2/CH_4$ mixture at a total flow rate of 50 sccm as a function of discharge power.

using our new comprehensive model (see Section 3), in comparison with experimental values obtained from ref 63, for a DBD in a 1:1 $CO_2/CH_4$ mixture at a total flow rate of 50 sccm. The $CH_4$ and $CO_2$ conversions both increase with discharge power, which is again logical, and the $CH_4$ conversion is about a factor 1.5 higher than the $CO_2$ conversion. Very good agreement is reached between calculated and experimental conversions.

*2.2.2. Artificial Photosynthesis and $CO_2$ Hydrogenation.* Research toward $CO_2$ conversion in the presence of $H_2O$ (artificial photosynthesis) and $H_2$ ($CO_2$ hydrogenation) is quite limited, and to our knowledge the only models available are developed within the research group PLASMANT.[73,74]

In Figure 4, the calculated absolute $CO_2$ and $H_2O$ conversions, as obtained from our new plasma chemistry model, are compared

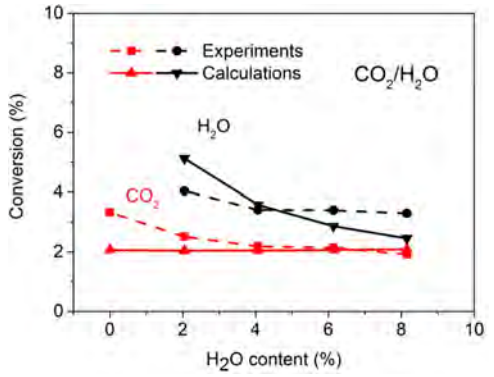


**Figure 4.** Comparison of the calculated absolute conversion of $CO_2$ and $H_2O$, as obtained from our new comprehensive plasma chemistry model, with measured data adopted from ref 73 in a $CO_2/H_2O$ mixture as a function of water vapor content for an SEI of 1.1 eV/molecule and a total flow rate of 600 mL/min at 323 K.

with experimental data for a DBD, as a function of water vapor content for a total gas flow rate of 600 mL/min at 323 K for an SEI value of 1.1 eV/molecule. Both the experimental and calculated absolute $H_2O$ conversions show a slightly decreasing trend with increasing water vapor content, although the drop is



DOI: 10.1021/acs.jpcc.7b10619
J. Phys. Chem. C 2018, 122, 8704−8723

more pronounced in the simulation results. This is probably due to some more complex processes taking place in the experiments as a result of water vapor, which could not be easily accounted for in the 0D plasma chemistry model. Indeed, the model does not take into account some physical effects, such as condensation and nebulization.[73] Furthermore, water cluster ions and surface processes, which might be important in a water discharge,[75] are not yet taken into account in our current model.

The experiments also show a slight drop in $CO_2$ conversion with increasing water content. As explained in ref 73, this may result from destabilization of the discharge induced by the presence of water. This trend is also not captured by the simulation, but the agreement is still reasonable because both simulations and experiments show that the addition of water vapor into $CO_2$ exerts only a weak influence on the $CO_2$ conversion.

**2.3. Effect of $N_2$ as Impurity and Admixture.** The modeling studies in the above two sections, and their experimental counterparts, are limited to high-purity gases, hence without the presence of impurities. However, in the real world, for which we are trying to design industrial applications, this will never be the case. $N_2$ will always be an important impurity or even admixture. This must be taken into account in modeling because it is known that $N_2$ can influence the plasma physics, and, moreover, $N_2$ has metastable states, which could influence the plasma chemistry. As a result, the next step in plasma chemistry modeling must be the inclusion of these real-world impurities into existing models.

*2.3.1. Effect of $N_2$ on $CH_4$ Reforming.* Few modeling studies exist in literature regarding the addition of $N_2$ to the $CH_4$ reforming process,[76−81] but to our knowledge, the research group PLASMANT was the only one focusing on both the impurity and admixture level.[81]

The values for the absolute conversion of $CH_4$, calculated with our new plasma chemistry model, are plotted versus $N_2$ content in Figure 5, showing a good agreement with measured results,

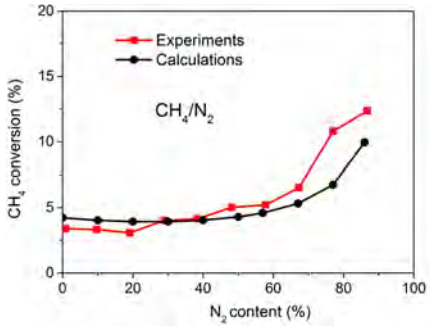


**Figure 5.** Comparison of the calculated absolute $CH_4$ conversion, as obtained from our new comprehensive plasma chemistry model, with measured data adopted from ref 81 in a $CH_4/N_2$ mixture as a function of $N_2$ content for a residence time of 2.2 s and an SEI of 1.5 eV/molecule.

obtained in a DBD, for a residence time of 2.2 s and an SEI of 1.5 eV/molecule.[81] Upon the addition of $N_2$, the absolute $CH_4$ conversion first remains more or less constant or even slightly decreases, and subsequently it increases. This trend results from the interplay of several effects; that is, the decreasing electron density with increasing $N_2$ content and the lower reaction rate constants for several three-body reactions with $N_2$ compared with $CH_4$ as third body cause a drop in absolute $CH_4$ conversion, but, on the contrary, $N_2$ can also enhance the absolute $CH_4$ conversion due to the dissociation of $CH_4$ upon collision with $N_2$ metastable molecules.

*2.3.2. Effect of $N_2$ on $CO_2$ Splitting.* Investigating the influence of $N_2$ present during the conversion of $CO_2$ is of vital importance because most $CO_2$ effluent gases contain large fractions of $N_2$, and the combined presence of N and O species is bound to lead to the formation of unwanted $NO_x$ byproducts. The only modeling studies performed here are from the research group PLASMANT.[82,83]

Figure 6 illustrates the absolute $CO_2$ conversion, calculated with the new plasma chemistry model, in comparison with our

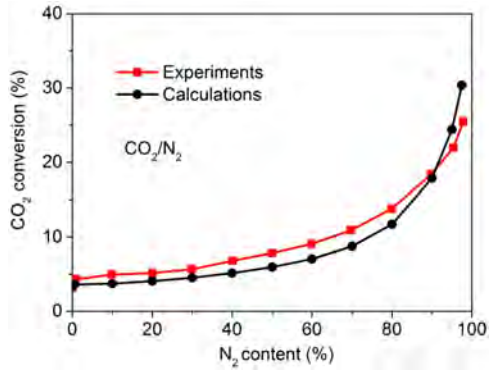


**Figure 6.** Comparison of the calculated absolute $CO_2$ conversion, as obtained from our new comprehensive plasma chemistry model, with measured data adopted from ref 83 in a $CO_2/N_2$ mixture as a function of $N_2$ content for a residence time of 0.73 s and an SEI of 3.0 eV/molecule.

previous experimental data,[83] in a $CO_2/N_2$ mixture as a function of the $N_2$ content for a residence time of 0.73 s and an SEI of 3.0 eV/molecule, showing again a very good agreement. The absolute $CO_2$ conversion increases more or less exponentially with rising $N_2$ fraction, both in the experiments and the calculations. This indicates that $N_2$ has a beneficial effect on $CO_2$ splitting due to the dissociation of $CO_2$ upon collision with $N_2$ metastable molecules (mainly $N_2(A^3\Sigma_u^+)$).

## 3. COMPREHENSIVE CHEMICAL KINETICS PLASMA MODEL

It is clear from the previous section that the new plasma chemistry model provides good agreement with our previous (published) experimental data for pure $CO_2$ as well as binary mixtures ($CO_2/CH_4$, $CO_2/H_2O$, $CH_4/N_2$, and $CO_2/N_2$), which serves as an important first validation. In this section we will present for the first time the combination of all of these chemistry models and validate it against new experimental data in multicomponent mixtures. The temperature-controlled coaxial DBD reactor used for these new experiments has been introduced in previous work.[84,85] This new comprehensive chemistry model can be used to investigate any desired multicomponent mixture, containing $CO_2$, $CH_4$, $N_2$, $O_2$, and $H_2O$ in its feed. We will start by giving a brief explanation of the model as well as an overview of the included plasma chemistry and how it was developed. Subsequently, we will look into the results of some multicomponent mixtures, that is, $CO_2/CH_4/N_2$, $CO_2/CH_4/N_2/O_2$, and $CO_2/CH_4/N_2/H_2O$. For these mixtures we will compare the calculated and measured conversions of $CO_2$ and $CH_4$ and the product selectivities at various gas mixing ratios for the purpose of validation. Indeed, the present (experimental) results were not optimized; they were only obtained under a fixed condition of flow rate and power, so not focusing on the highest conversion or product selectivities, but they only serve to validate the new


DOI: 10.1021/acs.jpcc.7b10619
J. Phys. Chem. C 2018, 122, 8704−8723

**Table 1. Overview of the Species Included in the Model**

| molecules | charged species | radicals | excited species |
|---|---|---|---|
| $C_3H_8$, $C_3H_6$, $C_2H_6$, $C_2H_4$, $C_2H_2$, $CH_4$ | $C_2H_6^+$, $C_2H_5^+$, $C_2H_4^+$, $C_2H_3^+$, $C_2H_2^+$, $C_2H^+$, $CH_5^+$, $CH_4^+$, $CH_3^+$, $CH_2^+$, $CH^+$ | $C_4H_2$, $C_3H_7$, $C_3H_5$, $C_2H_5$, $C_2H_3$, $C_2H$, $CH_3$, $CH_2$, $CH$ | |
| $CO_2$, $CO$ | $CO_2^+$, $CO^+$, $CO_3^-$, $CO_4^-$, $CO_4^+$, $C_2O_4^+$, $C_2O_3^+$, $C_2O_2^+$ | $C_2O$ | $CO_2$(e1), $CO_2$(e2) |
| $C_2N_2$ | | CN, NCN | |
| $H_2O$, $H_2O_2$ | $H_2O^+$, $H_3O^+$, $OH^+$, $OH^-$ | $HO_2$, OH | |
| $N_2H_4$, $NH_3$, $N_2H_2$ | $NH_4^+$, $NH_3^+$, $NH_2^+$, $NH^+$ | $NH_2$, NH, $N_2H$, $N_2H_3$ | |
| $N_2O$, $N_2O_3$, $N_2O_4$, $N_2O_5$ | $NO^+$, $N_2O^+$, $NO_2^+$, $NO^-$, $N_2O^-$, $NO_2^-$, $NO_3^-$, $O_2^+N_2$ | NO, $NO_2$, $NO_3$ | |
| $CH_2CO$, $CH_3OH$, $CH_3CHO$, $CH_3OOH$, $C_2H_5OH$, $C_2H_5OOH$, $CH_2O$ | | CHO, $CH_2OH$, $CH_3O$, $CH_3O_2$, $C_2HO$, $CH_3CO$, $CH_2CHO$, $C_2H_5O$, $C_2H_5O_2$ | |
| HCN | | $H_2CN$ | |
| | | ONCN, NCO | |
| | $C_2^+$, $C^+$ | C, $C_2$ | |
| $N_2$ | $N_2^+$, $N^+$, $N_3^+$, $N_4^+$ | N | $N_2(a'\Sigma_u^-)$, $N_2(C^3\Pi_u)$, $N_2$(V), $N_2(A^3\Sigma_u^+)$, $N_2(B^3\Pi_g)$ N(2P), N(2D) |
| $H_2$ | $H_2^+$, $H^+$, $H^-$, $H_3^+$ | H | H(2P), $H_2$(V), $H_2$(E) |
| $O_3$, $O_2$ | $O_3^-$, $O_4^-$, $O_4^+$, $O_2^-$, $O_2^+$, $O^+$, $O^-$ $e^-$ | O | O(1D), O(1S), $O_2$(a1), $O_2$(b1) |

chemical kinetics model. Finally, we will discuss in detail the underlying chemistry as predicted by the model to explain the observed trends in conversion and product selectivities.

**3.1. Plasma Chemistry Model.** There exist different types of models for non-LTE plasmas,[86−88] but the most straightforward approach to model a detailed plasma chemistry is a 0D chemical kinetics model, also called global model. It is based on solving balance equations for the densities of the various plasma species (i.e., various types of molecules, radicals, atoms, ions, excited species, and the electrons) based on production and loss terms, as defined by chemical reactions.[15,16] Details of the model that is used here to describe the plasma chemistry of $CO_2$ and $CH_4$ conversion in the multicomponent mixtures are presented in the Supporting Information.

As indicated in Section 2, within the PLASMANT group several different plasma chemistry models have been developed in the past 5 to 10 years, not only for gas conversion applications but also for other reactive gas mixtures. The most important chemistries used here for developing our new comprehensive plasma chemistry model for a DBD plasma are (i) the pure $CO_2$ chemistry model of Aerts et al.;[29,33] (ii) a model containing the $H_2O/O_2$ chemistry by Van Gaens et al.;[89] (iii) the interaction of $CO_2$ and $CH_4$ in the DRM process developed by De Bie et al.[65] and Snoeckx et al.;[63] (iv) a chemistry set describing the interaction between $CO_2$ and $H_2O$ in the work of Snoeckx et al.;[73] (v) a model containing the $CH_4/N_2$ chemistry by Snoeckx et al.;[81] and finally (vi) chemistry models describing the interaction in $CO_2/N_2$ plasmas by Heijkers et al.[82] and Snoeckx et al.[83] All of these different chemistry models were developed and used to investigate specific problems in combination with experiments for pure $CO_2$ splitting in humid air for dry reforming of methane, artificial photosynthesis, and the influence of $N_2$ on $CH_4$ reforming and on pure $CO_2$ splitting, respectively. We combine all of this knowledge from previous research on the different single-component, two-component, and impurity mixtures to arrive at a new comprehensive chemistry model, which can be used to investigate any desired multicomponent mixture containing $CO_2$, $CH_4$, $N_2$, $O_2$, and $H_2O$ in its feed. To achieve this, the chemistry from the above-mentioned models was adopted, adapted, and expanded with additional reactions. This led to a model containing 137 species, as listed in Table 1. Note that the model does not include vibrationally excited molecules, in contrast with other models developed within PLASMANT.[30−38,82] Indeed, the plasma chemistry model presented here is applied to a DBD plasma (see Section 2 and Figure 1), where vibrationally excited species are of minor importance.[33,35] In microwave (MW) or gliding arc (GA) discharges, however, vibrationally excited species are very important,[30−32,34−38,82] and thus the model would have to be extended to these species to account for their role in the conversion mechanisms (see Conclusions and Outlook).

These 137 species react with each other through 355 electron impact reactions, 631 ion reactions, and 743 neutral reactions. The full list of all of these reactions can be found in the Supporting Information, together with their corresponding rate coefficients and the references where these data were adopted from. The model itself is based on solving balance equations for all species densities, with production and loss terms defined by chemical reactions, as explained in the Supporting Information. In addition, a Boltzmann equation is used to calculate the rate coefficients of all of the electron impact reactions. The processes included in this Boltzmann equation are elastic collisions, electron impact vibrational excitation/de-excitation, electronic excitation/de-excitation (both dissociative and nondissociative), electron attachment, as well as electron impact ionization of various important species (see Table S1 in the Supporting Information).

As validation of this newly developed chemistry set, we compared the calculated conversions with measured values for different gas mixtures obtained from our previous work; see Figures 2−6. These simulations were performed for exactly the same operating conditions as in the experiments. Furthermore, additional experiments were performed for the new multicomponent mixture containing $CO_2$, $CH_4$, $N_2$, $O_2$,and $H_2O$, for extra validation of the new model, which will be presented below. For more details of the model and the additional experiments as well as the definitions of gas conversion and product selectivities, we refer to the Supporting Information.

**3.2. Plasma Conversion and Product Selectivity.** *3.2.1. $CO_2/CH_4/N_2$ Mixture: Varying $CO_2$ and $N_2$ Content.* Effluent gas flows from industrial and Carbon Capture Sequestration/Utilization/Recycling (CCS/U/R) often contain impurities, of



DOI: 10.1021/acs.jpcc.7b10619
J. Phys. Chem. C 2018, 122, 8704−8723

which in most cases $N_2$ is the main component. Therefore, it is of interest to study the $CO_2$ and $CH_4$ conversion in the presence of $N_2$. Figure 7 shows the measured and calculated absolute $CO_2$

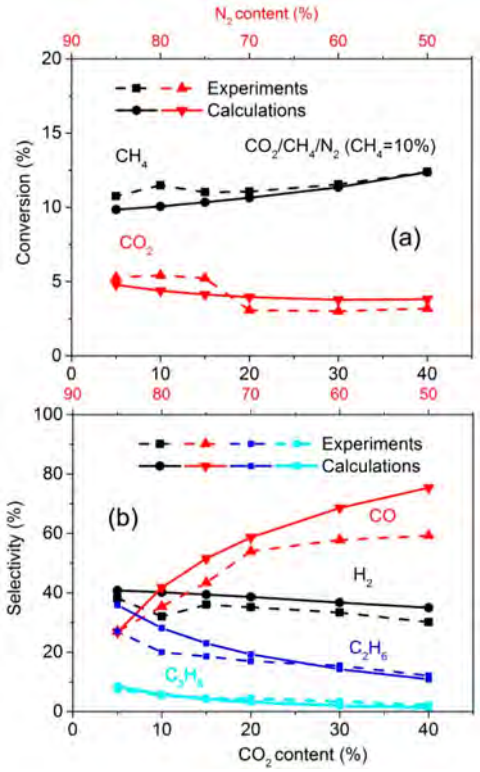


**Figure 7.** Comparison of the calculated and measured conversion of $CH_4$ and $CO_2$ (a) and selectivities of the most important products (b) in a $CO_2/CH_4/N_2$ mixture as a function of the $CO_2$ (and $N_2$) content for a fixed total flow rate of 200 mL/min and plasma power of 10 W, corresponding to an SEI of 0.76 eV/molecule. The $CH_4$ content was fixed at 10%, with the remainder being $CO_2$ and $N_2$.

and $CH_4$ conversions (a) and the product selectivities (b) plotted as a function of the $CO_2$ (and $N_2$) content in a $CO_2/CH_4/N_2$ mixture, keeping the $CH_4$ content fixed at 10%.

At all of the gas mixing ratios investigated, the $CH_4$ conversion is much higher than the $CO_2$ conversion. This can be explained because the rate of electron impact dissociation of $CH_4$ is higher than that of $CO_2$ due to the lower C−H bond dissociation energy. Although there is some small deviation in the exact trend with increasing $CO_2$ content, in general, the calculated values show reasonable agreement with the experiments.

The $CO_2/CH_4$ ratio has an important influence on the product selectivities, as is clear from Figure 7b. At low $CO_2/CH_4$ ratio ($CO_2$ content of 5%), the selectivities of the hydrocarbons (mainly $C_2H_6$) are comparable to or even slightly higher than that of CO. With increasing $CO_2/CH_4$ ratio, the selectivities of the hydrocarbons and $H_2$ steadily decrease, while the CO selectivity increases, which is logical as CO is the major product of $CO_2$ splitting, while the hydrocarbons and $H_2$ originate from $CH_4$ dissociation. Increasing the $CO_2/CH_4$ ratio from 0.5 to 4 yields a drop in the $H_2/CO$ ratio from 2.45 to 0.42. These results show that the $H_2/CO$ ratio can be varied in a wide range, simply controlled by the inlet gas mixing ratio. This is an advantage compared with classical processes, including steam reforming, partial oxidation, and $CO_2$ reforming, which typically produce syngas with $H_2/CO$ molar ratios of >3, <2, and <1, respectively.[90,91]

Finally, we conclude from Figure 7b that the calculated selectivities are in good agreement with the experiments.

*3.2.2. $CO_2/CH_4/N_2$ Mixture: Varying $N_2$ Content.* Figure 8 illustrates the effect of $N_2$ content on the experimental and

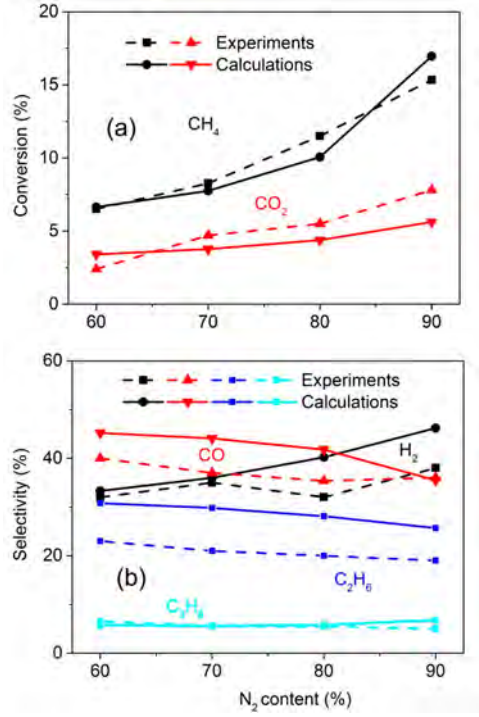


**Figure 8.** Comparison of the calculated and measured conversion of $CH_4$ and $CO_2$ (a) and selectivities of the most important products (b) in a $CO_2/CH_4/N_2$ mixture as a function of the $N_2$ content for a fixed 1:1 $CO_2/CH_4$ ratio, a fixed total flow rate of 200 mL/min, and a corresponding SEI of 0.76 eV/molecule.

calculated absolute $CO_2$ and $CH_4$ conversions (a) as well as on the product selectivities (b) keeping the $CO_2/CH_4$ ratio fixed at 1. Again, good agreement is reached between calculated and measured results, especially for the conversions. Figure 8a shows that increasing the $N_2$ content leads to a higher absolute conversion for both $CO_2$ and $CH_4$, in both the experimental and simulation results. This is mainly caused by the increasing role of the $N_2$ metastable states in the dissociation of both $CO_2$ and $CH_4$, as will be discussed in more detail in Section 3.3.

In our previous work, we investigated the effect of $N_2$ for both pure $CH_4$[81] and pure $CO_2$ splitting,[83] and in both cases the presence of $N_2$ led to unwanted effects, that is, soot deposition and $NO_x$ production, respectively. However, when combining both gases into the current $CO_2/CH_4/N_2$ mixture, no excessive soot deposition or $NO_x$ production is observed. This can be explained by the chemical kinetics model. Indeed, the O species, which react with N species to form $NO_x$ in the $CO_2/N_2$ mixture, form $H_2O$ in the presence of a hydrogen source due to the faster rates of the latter reactions. Vice versa, the O species prevent the occurrence of soot deposition by oxidation of the carbon containing species.

The major products in this $CO_2/CH_4/N_2$ mixture are again CO, $H_2$, $C_2H_6$, and $C_3H_8$. The measured and calculated selectivities show only a weak dependence on the $N_2$ content within the investigated range, except for the calculated $H_2$ selectivity, which clearly rises upon rising $N_2$ content, while the measured values show only a very weak increase. The calculated



DOI: 10.1021/acs.jpcc.7b10619
J. Phys. Chem. C 2018, 122, 8704−8723

CO, $H_2$, and $C_2H_6$ selectivities are somewhat higher than the experimental data, which might be attributed to the limitation of the 0D model, neglecting transport and surface reactions. The latter may become important under some conditions. In contrast, excellent agreement between calculations and experiments is reached for the $C_3H_8$ selectivity. In general, we consider the agreement between calculated and measured selectivities as fairly good, in view of the complex chemistry and the limitations of the 0D model.

It is worth mentioning that although the $CO_2/CH_4$ ratio is kept constant, the experimental and calculated syngas ($H_2$/CO) ratio slightly rises upon increasing $N_2$ content, that is, from 1.16 to 1.40 in the experiments and from 0.97 to 1.96 in the calculated values, as can be deduced from the rising $H_2$ selectivities and the decreasing CO selectivities in Figure 8b. The reason for the latter will be explained in Section 3.3.

*3.2.3. $CO_2/CH_4/N_2/O_2$ Mixture: Varying $O_2$ (and $N_2$) Content.* In literature, POX is widely used because $O_2$ is very effective for low-temperature plasma activation of methane. However, a possible drawback of POX is an excessive oxidation, resulting in the formation of $CO_2$. The use of $CO_2$ as a milder oxidant with a little addition of $O_2$ may combine the advantages of DRM and POX and have a positive influence on the products formed. Therefore, we also investigate the influence of $O_2$ addition on the $CO_2$ and $CH_4$ conversions, as well as on the product selectivities, as presented in Figure 9a,b, respectively.

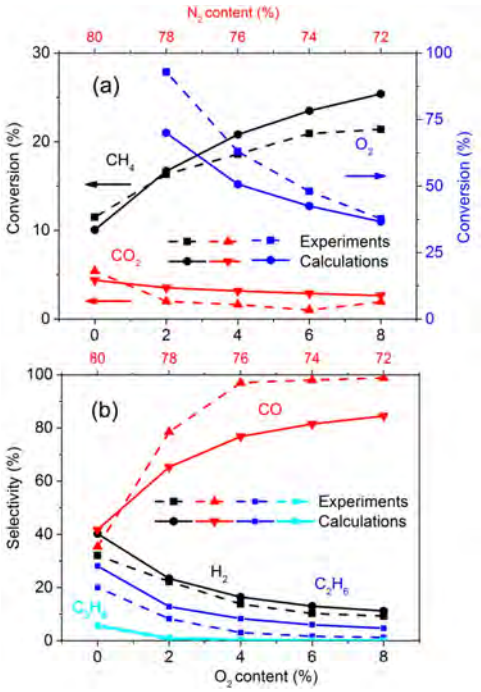


**Figure 9.** Comparison of the calculated and measured conversions of $CH_4$, $CO_2$, and $O_2$ (a) and selectivities of the most important products (b) in a $CO_2/CH_4/N_2/O_2$ mixture as a function of the $O_2$ (and $N_2$) content for a 1:1 $CO_2/CH_4$ ratio, a fixed total flow rate of 200 mL/min, and a corresponding SEI of 0.76 eV/molecule. The $CO_2$ and $CH_4$ content were both 10%, with the remainder being $O_2$ and $N_2$.

The addition of $O_2$ leads to a higher $CH_4$ conversion, while the $CO_2$ conversion decreases. Indeed, POX becomes the dominant process over DRM. As a result, part of the converted $CH_4$ is oxidized toward CO and $CO_2$, which explains the lower $CO_2$ conversion. The calculated $CH_4$ conversion is in good agreement with experiments, but there is some discrepancy for the $CO_2$ and $O_2$ conversion. This might be attributed to the occurrence of carbon deposition on the surface of the DBD reactor, which will be oxidized to CO and $CO_2$ by O species. Because the model does not take surface reactions into account, this process is neglected, which could explain the somewhat higher $CO_2$ conversion in the model than in the experiments. Furthermore, this may also explain the deviation in the calculated and measured $O_2$ conversion and the underestimated CO selectivity (see Figure 9b). However, we consider the agreement still as satisfactory, in view of the complex chemistry and limitations of the model.

Both the experiments and calculations show that the addition of $O_2$ rapidly decreases the selectivities of the hydrocarbons (mainly $C_2H_6$ and $C_3H_8$) and $H_2$ because of their oxidation into CO and $H_2O$. Indeed, the CO selectivity rises dramatically for the same reason. This also leads to a significant drop in the syngas ratio upon increasing $O_2$ content from 0 to 8%, that is, from 1.23 to 0.17 in the experiments, and from 1.34 to 0.25 in the calculations. Again, with some exceptions as explained above, quite good agreement is reached between the calculations and experiments.

*3.2.4. $CO_2/CH_4/N_2/H_2O$ Mixture: Varying $H_2O$ (and $N_2$) Content.* An interesting coreactant and hydrogen source for the conversion of $CO_2$ is $H_2O$. It is the most ubiquitous and cheapest hydrogen source available, especially compared with $CH_4$ and $H_2$. In addition, the combined conversion of $CO_2$ and $H_2O$ to produce value-added products using renewable energy would successfully mimic the natural photosynthesis process. Our previous study, however, revealed that this process is not an interesting one to pursue by means of plasma technology due to a severe drop in $CO_2$ conversion and energy efficiency when adding $H_2O$.[73] This was mainly attributed to the recombination of CO with OH into $CO_2$ as well as the recombination of H atoms with O atoms into OH and subsequently $H_2O$.[73,92]

However, from Figure 10a, it becomes clear that the combined conversion of $CH_4$ and $CO_2$ remains almost unchanged upon the addition of $H_2O$. Hence, the presence of $CH_4$ seems to counteract the negative effect of $H_2O$ addition because the H atoms originating from $CH_4$ dissociation can recombine with the OH radicals and thus suppress their negative effect, as there will be less OH available for the back reaction from CO to $CO_2$. Furthermore, the syngas ratio increases (from 1.35 to 1.65 in the experiments and from 1.34 to 1.50 in the model) upon increasing $H_2O$ content from 0 to 8%, which means that the added $H_2O$ is successfully converted into $H_2$ as well, and the formation of $H_2O$ from O and H atoms is limited due to Le Chatelier's principle.[93] Figure 10b shows that the selectivities of both $H_2$ and CO slightly increase with rising $H_2O$ content, indicating that $H_2O$ addition is beneficial for the production of syngas. Again, in general, good agreement is obtained between the experimental and calculated selectivities of the most important products as a function of the $H_2O$ content.

**3.3. Underlying Mechanisms of Plasma-based $CO_2$ and $CH_4$ Conversion.** Because the agreement between calculated and measured conversions and product selectivities is quite good, in a wide range of gas mixtures and mixing ratios, we can conclude that our chemical kinetics model can provide a realistic picture of the plasma chemistry of the DBD reactor for the multicomponent mixtures containing $CO_2$, $CH_4$, $N_2$, $O_2$, and $H_2O$ in its feed. Thus we can now discuss in more detail the underlying plasma chemistry, as predicted by the model, for both the $CO_2$ and $CH_4$ conversion as well as for the formation of CO, $H_2$, $C_2H_6$, and $C_3H_8$ in the presence of $N_2$. Similar results, but for the effect of $O_2$ and $H_2O$ addition, are presented in the SI. This is the most powerful aspect of plasma chemistry modeling. Indeed, a


DOI: 10.1021/acs.jpcc.7b10619
J. Phys. Chem. C 2018, 122, 8704−8723

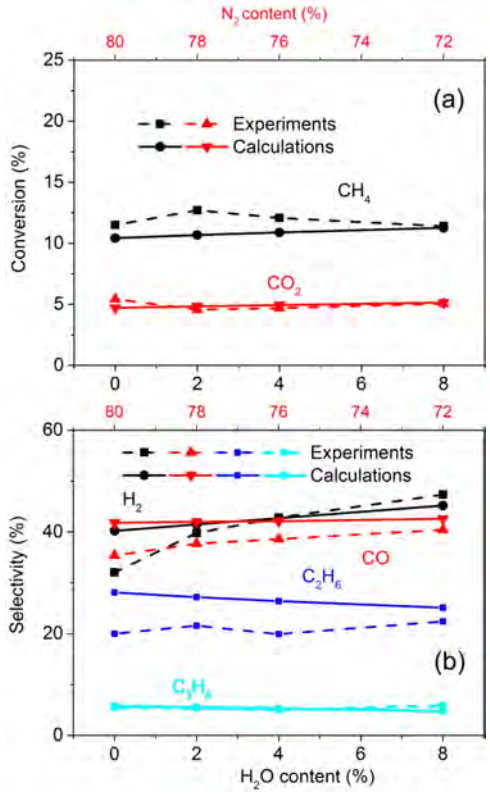


**Figure 10.** Comparison of the calculated and measured conversion of $CH_4$ and $CO_2$ (a) and selectivities of the most important products (b) in a $CO_2/CH_4/N_2/H_2O$ mixture as a function of the $H_2O$ (and $N_2$) content for a 1:1 $CO_2/CH_4$ ratio, a fixed total flow rate of 200 mL/min, and a corresponding SEI of 0.76 eV/molecule. The $CO_2$ and $CH_4$ content were both 10%, with the remainder being $H_2O$ and $N_2$.

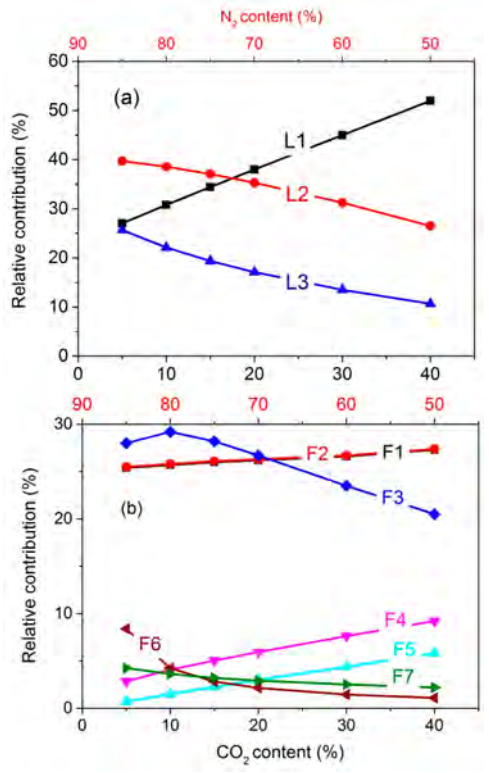


**Figure 11.** Relative contributions of the main processes leading to $CO_2$ loss (a) and formation (b) for a $CO_2/CH_4/N_2$ mixture as a function of the $CO_2$ (and $N_2$) content. The total flow rate is fixed at 200 mL/min and the plasma power is 10 W, corresponding to an SEI of 0.76 eV/molecule. The $CH_4$ content was fixed at 10%, with the remainder being $CO_2$ and $N_2$.

detailed analysis of the reaction pathways allows us to gain a better insight into the underlying chemical reactions and in the overall process. This, in turn, can help to optimize existing processes, overcome ongoing problems, find new research areas, and advance the steps toward a future industrial application of plasma-based gas conversion processes.

*3.3.1. $CO_2$ Conversion.* Table 2 lists the most important loss (L1–L3) and formation (F1–F9) processes for $CO_2$, and Figure 11 shows their relative contributions for a $CO_2/CH_4/N_2$ mixture. The $CH_4$ content was fixed at 10%, with the remainder being $CO_2$ and $N_2$. In the SI, we present similar results for a $CO_2/CH_4/N_2$ mixture at fixed $CO_2/CH_4$ ratio as well as upon the addition of $O_2$ or $H_2O$.

In the absence of $O_2$ and $H_2O$ (Figure 11) and at high $CO_2$ content (and thus low $N_2$ content), the most important dissociation reaction of $CO_2$, under the present DBD conditions, is electron impact dissociation (L1) into CO and O, while at low $CO_2$ content (and high $N_2$ content), the dissociation reaction with metastable $N_2(A^3\Sigma_u^+)$ molecules (L2) is dominant, yielding the same splitting products (CO and O). The reaction with metastable $N_2(B^3\Pi_g)$ molecules (L3) also has a non-negligible contribution to the dissociation of $CO_2$. Upon higher $N_2$ contents (lower $CO_2$ contents), the electron energy is gradually being used for $N_2$ excitation instead of $CO_2$ dissociation, explaining the drop in the relative contribution of electron impact dissociation and the corresponding increase in the relative

**Table 2. Dominant $CO_2$ Loss and Formation Reactions**

| process | loss reaction | process | formation reaction |
|---|---|---|---|
| L1 | $CO_2 + e^- \rightarrow e^- + CO + O$ | F1 | $CO + C_2O_3^+ + M \rightarrow CO_2 + C_2O_2^+ + M$ |
| L2 | $CO_2 + N_2(A^3\Sigma_u^+) \rightarrow N_2 + CO + O$ | F2 | $CO + C_2O_4^+ + M \rightarrow CO_2 + C_2O_3^+ + M$ |
| L3 | $CO_2 + N_2(B^3\Pi_g) \rightarrow N_2 + CO + O$ | F3 | $O + CH_3CO \rightarrow CO_2 + CH_3$ |
| | | F4 | $CO + OH \rightarrow CO_2 + H$ |
| | | F5 | $CO_3^- + C_2O_2^+ \rightarrow CO_2 + O + CO + CO$ |
| | | F6 | $CH_4 + CO_2^+ \rightarrow CO_2 + CH_4^+$ |
| | | F7 | $CO_3^- + H_3O^+ \rightarrow CO_2 + H_2O + H + O$ |
| | | F8 | $e^- + CO_4^+ \rightarrow CO_2 + O_2$ |
| | | F9 | $CH_2 + O_2 \rightarrow CO_2 + H + H$ |



DOI: 10.1021/acs.jpcc.7b10619
J. Phys. Chem. C 2018, 122, 8704–8723

**Table 3. Dominant $CH_4$ Loss and Formation Reactions**

| process | loss reaction | process | formation reaction |
|---|---|---|---|
| L1 | $CH_4 + e^- \rightarrow e^- + CH_3 + H$ | F1 | $CH_3 + H + M \rightarrow CH_4 + M$ |
| L2 | $CH_4 + CH \rightarrow C_2H_4 + H$ | F2 | $e^- + C_3H_8 \rightarrow CH_4 + e^- + C_2H_4$ |
| L3 | $CH_4 + N_2(a'\Sigma_u^-) \rightarrow N_2 + C + 2H_2$ | F3 | $CH_5^+ + H_2O \rightarrow CH_4 + H_3O^+$ |
| L4 | $CH_4 + N_2(A^3\Sigma_u^+) \rightarrow N_2 + CH_3 + H$ | | |
| L5 | $CH_4 + N_2(a'\Sigma_u^-) \rightarrow N_2 + CH_3 + H$ | | |
| L6 | $CH_4 + N_2(a'\Sigma_u^-) \rightarrow N_2 + CH_2 + H_2$ | | |
| L7 | $CH_4 + O \rightarrow CH_3 + OH$ | | |
| L8 | $CH_4 + OH \rightarrow CH_3 + H_2O$ | | |

contribution of dissociation by $N_2$ metastable molecules, which provides an alternative dissociation mechanism for $CO_2$. The same behavior can be seen in the $CO_2/CH_4/N_2$ mixture with fixed (1:1) $CO_2/CH_4$ ratio (see Figure S1a in the SI) and in the presence of $O_2$ (Figure S2a) as well as in the presence of $H_2O$ (Figure S3a in the SI). Thus at high $N_2$ content the major loss process of $CO_2$ is due to $N_2$ metastable states (reactions L2 and L3), and this explains why the presence of $N_2$ enhances the $CO_2$ conversion (see Figure 8).

If we take a look at the $CO_2$ formation in the $CO_2/CH_4/N_2$ mixture, the most significant processes are the ones between CO and the positive ions $C_2O_3^+$ and $C_2O_4^+$ through three-body reactions (F1, F2) as well as the neutral reactions between O atoms and $CH_3CO$ molecules (F3); see Figure 11b as well as Figure S1b in the SI. A similar conclusion can be obtained for the addition of $H_2O$ (Figure S3b in the SI).

With the addition of $O_2$, the behavior is a bit different. Indeed, the $CO_2/CH_4/O_2$ mixture gives rise to a high concentration of OH radicals. As a result, the reaction between CO and OH, leading to $CO_2$ and H atoms, becomes the dominant $CO_2$ formation process at $O_2$ contents above 5% (see Figure S2b: F4). This explains why the addition of $O_2$ leads to a decrease in $CO_2$ conversion, as indicated in Figure 9. This was also the case in our previous study for a $CO_2/H_2O$ mixture and resulted in a drop in $CO_2$ conversion upon $H_2O$ addition.[73] In the $CO_2/CH_4/N_2/H_2O$ mixture, however, the addition of $H_2O$ does not cause a drop in absolute $CO_2$ conversion, as presented in Figure 10, because the presence of $CH_4$, and thus H atoms, counteracts the negative effect of the OH radicals, as explained in Section 3.2.4.

Besides the recombination between CO and OH (F4), electron recombination with $CO_4^+$ (F8) and the reaction between $O_2$ and $CH_2$ (F9), which are quasi-negligible for $CO_2$ production in the other gas mixtures, also become important upon the addition of $O_2$ (Figure S2b). Other reactions involving ions (F5, F6, and F7) can also contribute to the $CO_2$ formation, but with a relative contribution of no more than 10%.

Finally, it is important to realize that the total formation rate of $CO_2$ is much smaller (no more than 10%) than the total $CO_2$ loss rate for a $CO_2/CH_4/N_2$ mixture as well as a $CO_2/CH_4/N_2/H_2O$ mixture, so the formation processes have only a minor contribution to the net $CO_2$ conversion under these conditions. However, the addition of $O_2$ enhances the formation of $CO_2$. With the addition of 8% $O_2$, the total $CO_2$ formation rate reaches 41% of the total $CO_2$ loss rate.

*3.3.2. $CH_4$ Conversion.* Table 3 lists the most important loss (L1−L8) and formation (F1−F3) processes for $CH_4$, and in Figure 12 the relative contributions of these processes are plotted as a function of $CO_2$ (and $N_2$) content in the $CO_2/CH_4/N_2$ mixture, at fixed $CH_4$ content of 10%, with the remainder being

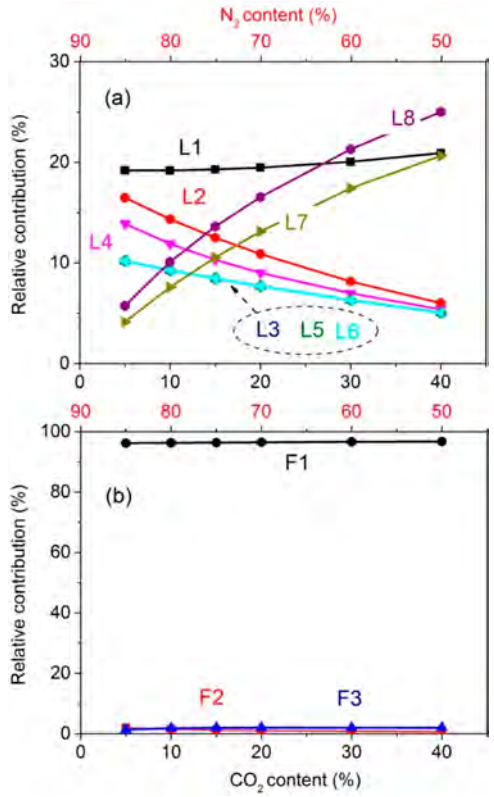


**Figure 12.** Relative contributions of the main processes leading to $CH_4$ loss (a) and formation (b) for a $CO_2/CH_4/N_2$ mixture as a function of the $CO_2$ (and $N_2$) content. The total flow rate is fixed at 200 mL/min and the plasma power is 10 W, corresponding to an SEI of 0.76 eV/molecule. The $CH_4$ content was fixed at 10%, with the remainder being $CO_2$ and $N_2$.

$CO_2$ and $N_2$. The results in the $CO_2/CH_4/N_2$ mixture with fixed $CO_2/CH_4$ ratio as well as upon the addition of $O_2$ or $H_2O$ are presented in Figures S4−S6 of the SI.

It is clear from Figure 12 that the dominant loss reactions change with increasing $CO_2$ content ($N_2$ content). Electron impact dissociation of $CH_4$ (L1) is always an important loss process under the present DBD conditions. It shows little dependence on the $CO_2$ content in Figure 12. The reaction between CH and $CH_4$ leading to $C_2H_4$ and H (L2) is also relatively important for $CH_4$ dissociation at low $CO_2$ content. The same applies for the reactions with $N_2$ metastable singlet and triplet states (reactions L3−L6 and especially L4).

Figure 12 shows that the dissociation process of $CH_4$ by metastable nitrogen molecules (L3+L4+L5+L6) could be more important than the direct electron impact processes (L1). The



DOI: 10.1021/acs.jpcc.7b10619
J. Phys. Chem. C 2018, 122, 8704−8723

**Table 4. Dominant CO Formation and Loss Reactions**

| process | formation reaction | process | loss reaction |
|---|---|---|---|
| F1 | $e^- + CO_2 \rightarrow CO + e^- + O$ | L1 | $CO + C_2O_3^+ + M \rightarrow C_2O_2^+ + CO_2 + M$ |
| F2 | $N_2(A^3\Sigma_u^+) + CO_2 \rightarrow CO + N_2 + O$ | L2 | $CO + C_2O_4^+ + M \rightarrow C_2O_3^+ + CO_2 + M$ |
| F3 | $CH_2O + O \rightarrow CO + OH + H$ | L3 | $CO + N \rightarrow CN + O$ |
| F4 | $N_2(B^3\Pi_g) + CO_2 \rightarrow CO + N_2 + O$ | L4 | $CO + CH + N_2 \rightarrow C_2HO + N_2$ |
| F5 | $H + CHO \rightarrow CO + H_2$ | L5 | $CO + H + M \rightarrow CHO + M$ |

rate coefficients of these processes are subject to some uncertainties, and this will affect the exact values of the relative contributions of these processes, predicted by the model. Nevertheless, we expect the general trends to be valid. Indeed, similar conclusions were made in literature[81] using the same reaction rate coefficients as in our work for the reactions with $N_2$ metastable singlet and triplet states (reactions L3−L6), and good agreement was reached with experiments, regardless of the conditions.

With increasing $CO_2$ content, the reactions between $CH_4$ and O atoms or OH radicals (L7 and L8) become increasingly important, and their relative contribution toward $CH_4$ loss even exceeds the contribution of electron impact dissociation (L1) at the highest $CO_2$ contents (and lowest $N_2$ contents) investigated. It should be noted that electron impact vibrational excitation of $CH_4$ is also important as loss process for the $CH_4$ ground-state molecules, but this process is only taken into account in our model as energy loss for the electrons and not as a chemical loss process for $CH_4$ because the vibrationally excited species are not considered separately in our model. Indeed, electron impact vibrational excitation mainly takes place in the lower electron energy range, and thus it is of lower importance when the reduced electric field (i.e., ratio of electric field over gas density) is quite high, such as in a DBD plasma.[33]

In the $CO_2/CH_4/N_2$ mixture with fixed 1:1 $CO_2/CH_4$ ratio, a similar behavior is observed (see Figure S4a in the SI), except that the relative contribution of electron impact dissociation clearly drops upon increasing $N_2$ content because of the drop in $CH_4$ content. With high $N_2$ content, the dissociation of $CH_4$ due to collisions with $N_2$ metastable states (reactions L3−L6) becomes most important, explaining why the presence of $N_2$ enhances the $CH_4$ conversion (see Figure 8).

Upon the addition of $O_2$ to the mixture, the loss reaction of $CH_4$ with OH radicals (L8) is dominant (Figure S5a in the SI). Its relative contribution gradually increases with higher $O_2$ contents because the concentration of produced OH radicals rises during both the microdischarge filaments and afterglow stages of the DBD. The same applies, to a lower extent, for the loss reaction upon collision with O atoms (L7). This explains why the $CH_4$ conversion rises drastically upon increasing $O_2$ content (see Figure 9).

$H_2O$ addition has no significant effect on the relative contributions of the various loss processes, except that the reaction with $N_2$ metastable triplet states $N_2(A^3\Sigma_u^+)$ (L4) drops and the reaction with OH radicals (L8) rises (see Figure S6a in the SI) due to a decreasing concentration of $N_2(A^3\Sigma_u^+)$ and increasing concentration of OH radicals, respectively.

If we take a look at the formation processes, the three-body recombination of $CH_3$ radicals with H atoms (F1) is the dominant formation process under all of the investigated conditions (see Figure 12b as well as Figures S4b, S5b, and S6b in the SI). Other reactions, such as electron impact dissociation of $C_3H_8$ into $CH_4$ (F2) and charge transfer between $H_2O$ and $CH_5^+$ (F3), have relative contributions of <5% to the $CH_4$ formation.

If we compare the total formation rate with the total loss rate of $CH_4$, we can conclude that the total formation rate is relatively large (up to 40%) compared with the total $CH_4$ loss rate, at least without $O_2$ addition. Hence, this behavior is different from the $CO_2$ loss and formation rates, as mentioned above. The reason is that the three-body recombination of $CH_3$ radicals with H atoms is very important outside the microdischarge filaments in the DBD reactor (see the SI for more details on how the microdischarge filaments in the DBD are treated; they are treated as afterglow in between discharge pulses). A similar behavior was reported by Snoeckx et al.[63] However, upon $O_2$ addition, the formation processes have a decreasing contribution to the net $CH_4$ conversion (formation rate of no more than 10% of the total $CH_4$ loss rate with 8% $O_2$ addition), explaining again why the $CH_4$ conversion drastically rises upon $O_2$ addition (see Figure 9).

*3.3.3. CO Production.* Because CO is the major product of the $CO_2$ conversion, with a selectivity of about 30−100% (see Figures 7−10), we present here the dominant reaction pathways for the formation and loss of CO, to obtain a better understanding of the influence of the $CO_2/CH_4$ ratio, the $N_2$ content, and the addition of $O_2$ or $H_2O$ on the CO yield. Table 4 lists the most important formation (F1−F5) and loss (L1−L7) processes for CO. Their relative contributions in the $CO_2/CH_4/N_2$ mixture are plotted in Figure 13 as a function of the $CO_2$ (and $N_2$) content. The corresponding results at fixed $CO_2/CH_4$ ratio, as well as upon the addition of $O_2$ or $H_2O$, are presented in Figures S7−S9 of the SI.

Electron impact dissociation of $CO_2$ (F1), as well as dissociation of $CO_2$ upon collision with $N_2$ metastable singlet and triplet states (F2 and F4), is the dominant formation process of CO under all conditions investigated (see Figure 13a and Figures S7a and S9a in the SI), except upon the addition of $O_2$. Furthermore, the reaction between $CH_2O$ and O, leading to CO, OH, and H (F3), also plays a quite important role, and this process even becomes the prime source of CO when $O_2$ is added (see Figure S8a in the SI). This additional channel for CO production explains why the addition of $O_2$ leads to a drastic increase in CO selectivity (see Figure 9).

As far as the loss of CO is concerned, the three-body reactions between CO and the positive ions $C_2O_3^+$ and $C_2O_4^+$ (L1, L2) are dominant under all conditions (see Figure 13b and Figures S7b and S9b in the SI), except upon the addition of $O_2$. These two reactions are also the most important for $CO_2$ formation (see Section 3.3.1). Upon the addition of $O_2$, however, the reaction of CO with OH becomes the most important route toward CO loss (L6, in Figure S8b), which is also the dominant process of $CO_2$ formation under these conditions.

Besides the CO loss reactions toward $CO_2$ formation (L1, L2, L6, L7), other loss channels include the reaction of CO with N, leading to CN and O (L3), the reaction with CH, leading to $C_2HO$



DOI: 10.1021/acs.jpcc.7b10619
J. Phys. Chem. C 2018, 122, 8704−8723

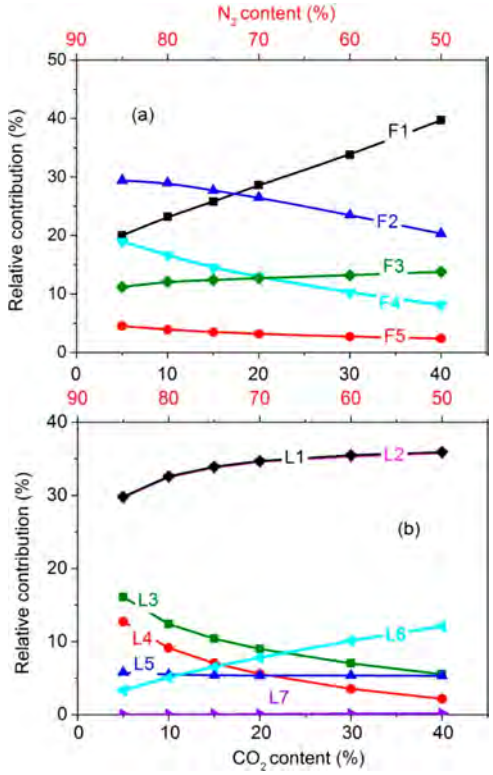


**Figure 13.** Relative contributions of the main processes leading to CO formation (a) and loss (b) for a $CO_2/CH_4/N_2$ mixture as a function of the $CO_2$ (and $N_2$) content. The total flow rate is fixed at 200 mL/min and the plasma power is 10 W, corresponding to an SEI of 0.76 eV/molecule. The $CH_4$ content was fixed at 10%, with the remainder being $CO_2$ and $N_2$.

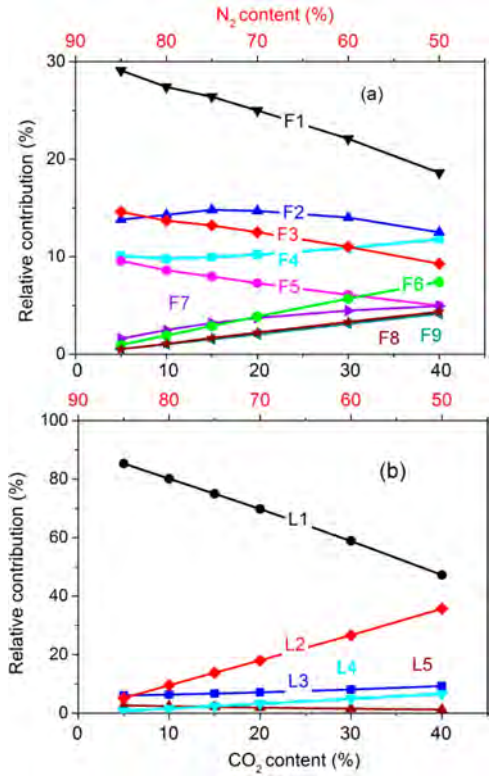


**Figure 14.** Relative contributions of the main processes leading to $H_2$ formation (a) and loss (b) for a $CO_2/CH_4/N_2$ mixture as a function of the $CO_2$ (and $N_2$) content. The total flow rate is fixed at 200 mL/min and the plasma power is 10 W, corresponding to an SEI of 0.76 eV/molecule. The $CH_4$ content was fixed at 10%, with the remainder being $CO_2$ and $N_2$.

(L4), and the reaction with H, producing CHO (L5), which have relative contributions up to 20% under the conditions investigated.

Finally, it is important to realize that the total loss rate of CO is much smaller (no more than 6%) than the total CO formation rate for all gas mixtures and mixing ratios investigated, so the loss processes only have a minor contribution to the net CO formation under these conditions.

*3.3.4. $H_2$ Production.* $H_2$ is also a significant product, due to the $CH_4$ conversion, with a selectivity of about 10−50% (see Figures 7−10). Table 5 lists the most important formation (F1−F9) and loss (L1−L5) processes for $H_2$, and Figure 14 illustrates the relative contributions of these processes for the $CO_2/CH_4/N_2$ mixture at constant $CH_4$ content. The results for the other conditions can be found in Figures S10−S12 in the SI.

The most important production process at all conditions investigated is the reaction of $CH_4$ with $N_2(a'\Sigma_u^-)$ metastable singlet states, producing C atoms and two $H_2$ molecules (F1). This reaction, of course, becomes increasingly important with increasing $N_2$ content. Furthermore, electron impact dissociation of $C_2H_6$ (F4) is an important formation process at lower $N_2$ content (see especially Figure S10a). The reaction of $CH_4$ with $N_2(a'\Sigma_u^-)$ toward the production of $CH_2$ radicals and one $H_2$ molecule (F3) also contributes to the $H_2$ production to some extent as well as the reaction of $H_2CN$, $CH_2$ radicals, CHO, and $CH_3OH$ with H (reactions F2, F5−F8) and the reaction of $CH_3$ with O atoms (F9) depending on the conditions.

The dominant loss process is the reaction of $H_2$ with a C atom producing a CH radical and a H atom (L1) at all gas mixing ratios

**Table 5. Dominant $H_2$ Formation and Loss Reactions**

| process | formation reaction | process | loss reaction |
|---|---|---|---|
| F1 | $N_2(a'\Sigma_u^-) + CH_4 \rightarrow 2H_2 + N_2 + C$ | L1 | $H_2 + C \rightarrow CH + H$ |
| F2 | $H_2CN + H \rightarrow H_2 + HCN$ | L2 | $H_2 + OH \rightarrow H_2O + H$ |
| F3 | $N_2(a'\Sigma_u^-) + CH_4 \rightarrow H_2 + N_2 + CH_2$ | L3 | $H_2 + e^- \rightarrow e^- + H + H$ |
| F4 | $e^- + C_2H_6 \rightarrow H_2 + e^- + C_2H_4$ | L4 | $H_2 + O \rightarrow OH + H$ |
| F5 | $CH_2 + H \rightarrow H_2 + CH$ | L5 | $H_2 + N(2P) \rightarrow NH + H$ |
| F6 | $CH_3OH + H \rightarrow H_2 + CH_2OH$ | | |
| F7 | $CHO + H \rightarrow H_2 + CO$ | | |
| F8 | $CH_3OH + H \rightarrow H_2 + CH_3O$ | | |
| F9 | $CH_3 + O \rightarrow H_2 + CO + H$ | | |



DOI: 10.1021/acs.jpcc.7b10619
J. Phys. Chem. C 2018, 122, 8704−8723

**Table 6. Dominant $C_2H_6$ Formation and Loss Reactions**

| process | formation reaction | process | loss reaction |
|---|---|---|---|
| F1 | $CH_3 + CH_3 + M \rightarrow C_2H_6 + M$ | L1 | $C_2H_6 + e^- \rightarrow e^- + C_2H_4 + H_2$ |
| F2 | $C_2H_5 + H + M \rightarrow C_2H_6 + M$ | L2 | $C_2H_6 + OH \rightarrow C_2H_5 + H_2O$ |
| F3 | $C_2H_5 + CH_3O \rightarrow C_2H_6 + CH_2O$ | L3 | $C_2H_6 + O \rightarrow C_2H_5 + OH$ |
| F4 | $C_2H_5 + CHO \rightarrow C_2H_6 + CO$ | L4 | $C_2H_6 + N_2(a'\Sigma_u^-) \rightarrow N_2 + C_2H_4 + H_2$ |
| F5 | $C_2H_5 + C_2H_5 \rightarrow C_2H_6 + C_2H_4$ | L5 | $C_2H_6 + N_2(A^3\Sigma_u^+) \rightarrow N_2 + C_2H_4 + H_2$ |
| | | L6 | $C_2H_6 + e^- \rightarrow e^- + C_2H_5 + H$ |
| | | L7 | $C_2H_6 + CH_2 \rightarrow C_3H_8$ |

(see Figure 14b and Figures S10b and S12b of the SI), except upon the addition of $O_2$ (see Figure S11b in the SI). The relative contribution of this reaction, however, rapidly drops with increasing $CO_2$ content because the C atom density decreases due to reaction with O-containing species, such as OH and $O_2$, which are directly or indirectly formed from $CO_2$. This also explains why the loss reaction with OH radicals (L2) becomes gradually more important upon rising $CO_2$ content (see Figure 14b). The latter reaction is also dominant upon the addition of $O_2$ (see Figure S11b of the SI) for the same reason. The increasing role of reaction L2 in the loss of $H_2$ also explains why the selectivity of $H_2$ decreases upon the addition of either $CO_2$ or $O_2$ (see Figures 7 and 9). Other reactions, including electron impact dissociation of $H_2$ (L3), oxidization of $H_2$ by O atoms generating OH and H (L4), and the reaction of $H_2$ with excited N atoms toward NH (L5), can also contribute to $H_2$ loss, but their relative contributions do not exceed 20% under the conditions investigated.

Finally, the total loss rate of $H_2$ ranges from 13 to 24% of the total $H_2$ formation rate for all gas mixtures and mixing ratios investigated, so the loss processes have a non-negligible contribution to the net $H_2$ formation under these conditions. In particular, $O_2$ addition enhances the total loss rate of $H_2$ via reaction L2, as mentioned above.

*3.3.5. $C_2H_6$ Production.* Table 6 lists the most important formation (F1–F5) and loss (L1–L7) processes for $C_2H_6$. In Figure 15, the relative contributions of these processes are plotted for a $CO_2/CH_4/N_2$ mixture at fixed $CH_4$ content. The results under the other conditions are given in Figures S13–S15 of the SI.

The dominant formation channel for $C_2H_6$ in all gas mixtures is three-body recombination of two $CH_3$ radicals (F1), contributing for >60% to the $C_2H_6$ formation and even up to 95% upon the addition of $O_2$. Upon the addition of $CO_2$ and $O_2$, the $CH_3$ radicals are consumed by other competitive channels involving oxygen-containing species, and this explains why the $C_2H_6$ selectivity gradually decreases with the addition of $CO_2$ and $O_2$ (see Figures 7 and 9). The second most important reaction is three-body recombination of $C_2H_5$ with H (F2), while the other recombination reactions of $C_2H_5$ with $CH_3O$, CHO, and $C_2H_5$ (F3–F5) are of minor importance.

The dominant loss reaction for $C_2H_6$ at nearly all conditions investigated is electron impact dissociation into $C_2H_4$ and $H_2$ (L1). The reaction of $C_2H_6$ with OH or O toward the production of $C_2H_5$ (L2–L3) is also relatively important; see especially Figures S13b and S14b. Indeed, upon the addition of $O_2$, L2 even becomes dominant (see Figure S14b). Finally, the dissociation of $C_2H_6$ upon collision with $N_2$ metastable molecules (both $N_2(a'\Sigma_u^-)$ and $(N_2A^3\Sigma_u^+)$) (L4 and L5) becomes gradually more important upon rising $N_2$ content, as expected. This explains why

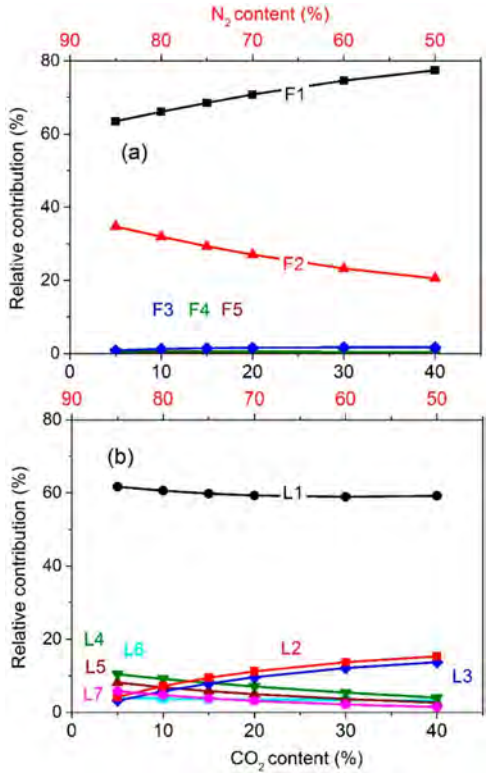


**Figure 15.** Relative contributions of the main processes leading to $C_2H_6$ formation (a) and loss (b) for a $CO_2/CH_4/N_2$ mixture as a function of the $CO_2$ (and $N_2$) content. The total flow rate is fixed at 200 mL/min and the plasma power is 10 W, corresponding to an SEI of 0.76 eV/molecule. The $CH_4$ content was fixed at 10%, with the remainder being $CO_2$ and $N_2$.

the $C_2H_6$ selectivity slightly decreases upon increasing $N_2$ content in Figure 8.

Finally, the total loss rate of $C_2H_6$ is 42 to 60% of the total $C_2H_6$ formation rate for all gas mixtures and mixing ratios investigated, so the loss processes have a quite large contribution to the net $C_2H_6$ formation under these conditions. Like for $H_2$, increasing the $O_2$ content enhances the total loss rate of $C_2H_6$.

*3.3.6. $C_3H_8$ Production.* Table 7 lists the most important formation (F1–F3) and loss (L1–L3) processes for $C_3H_8$, while the relative contributions of these processes for a $CO_2/CH_4/N_2$ mixture at constant $CH_4$ content are plotted in Figure 16. The results for the other gas mixtures are again presented in the SI (Figures S16–S18).

Three-body recombination of $C_2H_5$ and $CH_3$ radicals (F1) is the most important formation process. It contributes >70% under all conditions investigated and even up to 90% upon the addition



DOI: 10.1021/acs.jpcc.7b10619
J. Phys. Chem. C 2018, 122, 8704–8723

**Table 7. Dominant $C_3H_8$ Formation and Loss Reactions**

| process | formation reaction | process | loss reaction |
|---|---|---|---|
| F1 | $CH_3 + C_2H_5 + M \rightarrow C_3H_8 + M$ | L1 | $C_3H_8 + e^- \rightarrow e^- + C_3H_6 + H_2$ |
| F2 | $C_2H_6 + CH_2 \rightarrow C_3H_8$ | L2 | $C_3H_8 + e^- \rightarrow e^- + C_2H_4 + CH_4$ |
| F3 | $C_3H_7 + H \rightarrow C_3H_8$ | L3 | $C_3H_8 + e^- \rightarrow e^- + C_3H_7 + H$ |

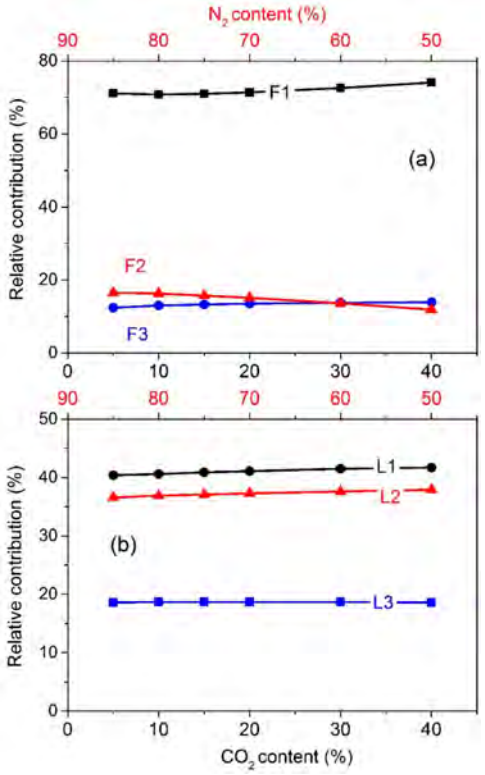


**Figure 16.** Relative contributions of the main processes leading to $C_3H_8$ formation (a) and loss (b) as a function of the $CO_2$ (and $N_2$) content for a fixed total flow rate of 200 mL/min and plasma power of 10 W, corresponding to an SEI of 0.76 eV/molecule. The $CH_4$ content was fixed at 10%, with the remainder being $CO_2$ and $N_2$.

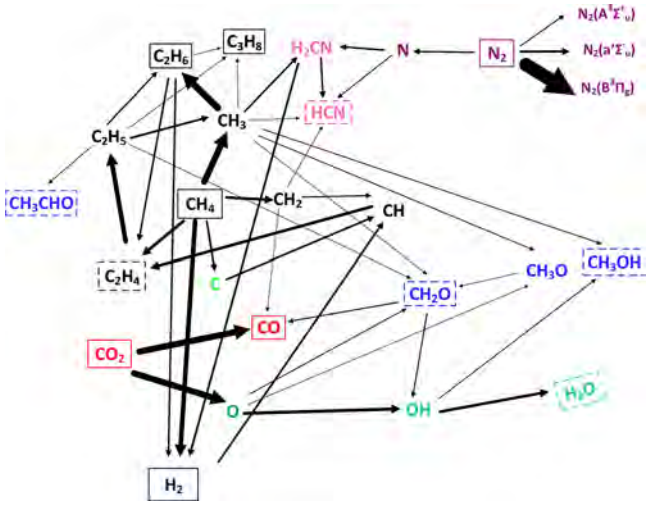


**Figure 17.** Schematic overview of the dominant reaction pathways for the conversion of $CH_4$ and $CO_2$ as well as $N_2$ in a 1:1:8 $CO_2/CH_4/N_2$ mixture for a fixed total flow rate of 200 mL/min and plasma power of 10 W, corresponding to an SEI of 0.76 eV/molecule. The thickness of the arrow lines is linearly proportional to the rate of the net reactions. The most important molecules are indicated with a solid line frame, the molecules formed with lower densities are written in a frame with dashed lines, while the radicals are not written in a frame.

of $O_2$ (Figure S17a). Finally, the loss of $C_3H_8$ occurs almost entirely through electron impact dissociation (L1−L3 in decreasing order of importance) under all conditions investigated.

Finally, our calculations reveal that the loss of $C_3H_8$ is quite significant compared with their production because the total loss rate takes up around 38 to 46% of the total formation rate.

*3.3.7. General Overview of the Reaction Pathways.* From the above detailed analysis of the dominant loss and formation reactions for $CH_4$, $CO_2$, and the major products, we can compose a general picture of the dominant reaction pathways in the plasma. This is summarized in Figure 17 for a 1:1:8 $CO_2/CH_4/N_2$ mixture at a fixed total flow rate of 200 mL/min and plasma power of 10 W, corresponding to an SEI of 0.76 eV/molecule.

The conversion process, under the present DBD conditions, starts with electron impact dissociation of $CH_4$, forming $CH_3$ radicals. Meanwhile, electron impact excitation of $N_2$ produces metastable singlet and triplet states, which also promote the dissociation of $CH_4$ toward $CH_3$, $CH_2$, CH radicals, and C atoms. The $CH_3$ radicals will recombine toward higher hydrocarbons, that is, mainly $C_2H_6$ and $C_3H_8$. Moreover, the recombination between $CH_4$ and CH produces unsaturated hydrocarbons, that is, mainly $C_2H_4$. The latter can recombine with H atoms into $C_2H_5$ radicals, which further produce other hydrocarbons, such as $C_2H_6$ and $C_3H_8$, as well as $CH_3$ radicals. Furthermore, dissociation of $CH_4$ and the higher hydrocarbons by electron impact and by collisions with $N_2$ metastable states yields the formation of $H_2$.

At the same time, electron impact collisions with $N_2$ also yield splitting of $N_2$ into N atoms, which can react with $CH_3$ radicals to generate $H_2CN$. The latter are not stable and quickly transform into hydrogen cyanide (HCN) upon impact with N or H atoms. At 80% $N_2$ content, our simulation shows that HCN is the most abundant N-containing end product (~1600 ppm). This indicates that the presence, even in high concentrations, of $N_2$ does not result in a significant production of N-containing species. This is in qualitative agreement with our experiments because no N-containing species were detected.

Electron impact dissociation and dissociation upon impact with $N_2$ metastable states also contribute to the conversion of $CO_2$ into CO and O. Moreover, the $CH_3$ radicals, formed by $CH_4$ dissociation, react with O atoms to form $CH_2O$ (formaldehyde) and $CH_3O$ radicals. The latter can subsequently be converted into $CH_2O$ as well. Furthermore, the O atoms can react with $CH_2O$ or $CH_4$ to produce OH radicals, which can further react with $CH_3$ radicals into $CH_3OH$ (methanol), albeit to a lower extent. The OH radicals also react further into $H_2O$. Finally, the O atoms, created from $CO_2$ conversion, initiate the formation of other oxygenates, like acetaldehyde ($CH_3CHO$). However, this reaction path is not so important because of the limited formation of O radicals.

In order of decreasing importance, $H_2$, CO, $C_2H_6$, $H_2O$ as well as the hydrogen cyanide (HCN) are the main end products (with



DOI: 10.1021/acs.jpcc.7b10619
J. Phys. Chem. C 2018, 122, 8704−8723

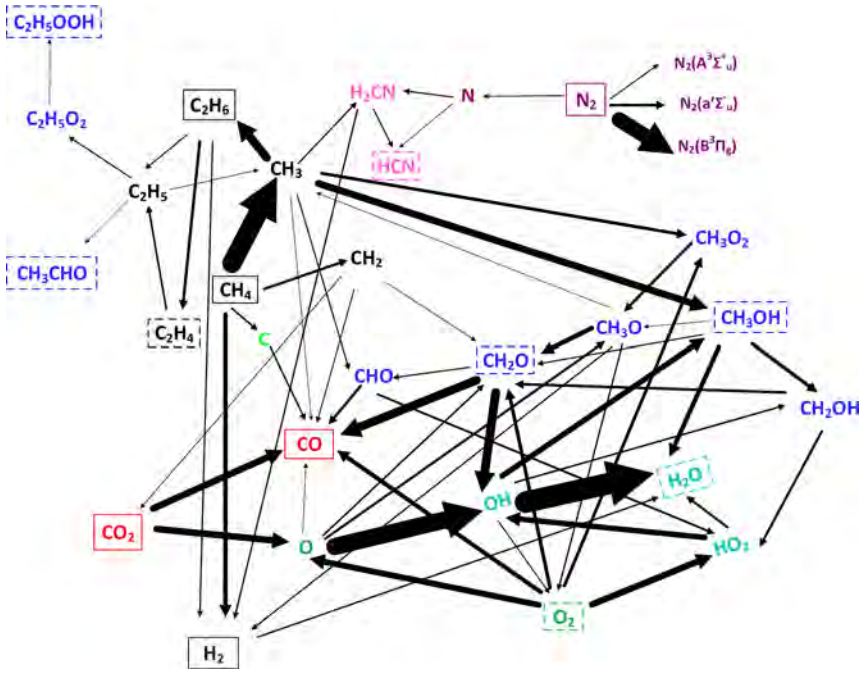


**Figure 18.** Schematic overview of the dominant reaction pathways for the conversion of $CH_4$, $CO_2$, $O_2$, and $N_2$ in a 10:10:78:2 $CO_2/CH_4/N_2/O_2$ mixture for a fixed total flow rate of 200 mL/min and plasma power of 10 W, corresponding to an SEI of 0.76 eV/molecule. The thickness of the arrow lines is linearly proportional to the rate of the net reactions. The most important molecules are indicated with a solid line frame, the molecules formed with lower densities are written in a frame with dashed lines, while the radicals are not written in a frame.

molar fractions of 0.80, 0.60, 0.20, 0.19, and 0.16%, respectively) in a 1:1:8 $CO_2/CH_4/N_2$ mixture. The fraction of other oxygenates ($CH_2O$, $CH_3OH$, etc.) as well as $C_3H_8$ in the end products is <0.1%, and hence their yields are of minor importance. Note that HCN was not detected in our experiments, although the calculations predict a higher concentration than for $C_3H_8$. This is because thermal conductivity detectors (TCDs) and a flame-ionization detector (FID) were used to detect the products. These detectors are more sensitive and hence have a much lower detection limit for $C_3H_8$ compared with HCN. Moreover, the yield of water ($H_2O$) was not calculated in the experiments because GC measurements are not suitable to deliver quantitative data about $H_2O$.

Our previous study showed that the presence of $N_2$ during $CO_2$ splitting leads to the formation of $N_2O$ and several $NO_x$ compounds, with concentrations in the range of several 100 ppm.[83] These concentrations are too low to be considered useful for nitrogen fixation[6,7] but will give rise to several environmental problems. $N_2O$ is an even more potent greenhouse gas than $CO_2$, with a global warming potential (GWP) of 298 $CO_2$-equivalent, while NO and $NO_2$ are responsible for acid rain and the formation of ozone and a wide variety of toxic products. However, our calculations predict that with the addition of $CH_4$, the production of $NO_x$ compounds upon reaction between N and O species is prohibited because of the faster reaction between O and H species, as explained in Section 3.2. Therefore, no $NO_x$ compounds are plotted in Figure 17. This result is very important because it indicates that DRM in a real gas effluent, containing significant amounts of $N_2$, would not cause problems of $NO_x$ formation, which are present in $CO_2$ splitting upon the addition of $N_2$.

From the analysis of the dominant loss and formation processes in Sections 3.3.1−3.3.6, it became clear that the addition of water does not change the plasma chemistry to a large extent because of its limited influence on the $CH_4$ and $CO_2$ conversion (see also Figure 10). Hence, the dominant reaction pathways in a $CO_2/CH_4/N_2/H_2O$ mixture are also well represented by Figure 17.

For the $CO_2/CH_4/N_2/O_2$ mixture, on the contrary, the situation is different because $O_2$ addition affects the dominant loss and formation reactions, as was clear from Sections 3.3.1−3.3.6. Therefore, we plot in Figure 18 the dominant reaction pathways for the conversion of $CH_4$, $CO_2$, $O_2$, and $N_2$ in a 10:10:78:2 $CO_2/CH_4/N_2/O_2$ mixture. Again, electron impact dissociation of $CH_4$ and dissociation upon impact with $N_2$ metastable singlet and triplet states result in the formation of $CH_3$ radicals. The latter can again recombine into hydrocarbons, such as ethane ($C_2H_6$), but the production of higher hydrocarbons through $CH_3$ recombination is reduced due to the increased recombination rate between $CH_3$ and $O_2$ or OH radicals, which are more abundant in the case of $O_2$ addition, yielding methanol ($CH_3OH$) formation. Moreover, the recombination of $CH_3$ radicals and $O_2$ molecules into $CH_3O_2$ radicals, which further form $CH_3O$, also becomes important. The $CH_3O$ radicals also yield the formation of formaldehyde ($CH_2O$) and methanol ($CH_3OH$). However, methanol ($CH_3OH$) can quickly react back into $CH_3O$ radicals through the reverse reactions with O, H, or OH radicals at a somewhat larger rate, so our model reveals a net conversion from methanol ($CH_3OH$) to formaldehyde ($CH_2O$).

In addition, methanol ($CH_3OH$) can react further into formaldehyde ($CH_2O$) through the $CH_2OH$ radicals, and formaldehyde ($CH_2O$) can further be converted into CO, either directly upon reaction with O atoms or indirectly through the CHO radicals. Furthermore, the reaction of formaldehyde ($CH_2O$) with O atoms also produces OH radicals. The $O_2$ molecules are converted into $HO_2$ radicals, O atoms, and CO as well as formaldehyde ($CH_2O$). It is worth mentioning that most of the $O_2$ conversion proceeds through collisions between neutral species. For instance, $O_2$ dissociation upon impact with $N_2$ metastable states contributes for ∼15%, showing the important role



DOI: 10.1021/acs.jpcc.7b10619
J. Phys. Chem. C 2018, 122, 8704−8723

of $N_2$, while electron impact dissociation contributes for only 3 to 4%.

CO can be further oxidized into $CO_2$ upon reaction with OH radicals. Furthermore, also the $CH_2$ radicals can be oxidized into $CO_2$. These reactions are obviously undesired. The O atoms are also converted into $CH_3O$ and OH radicals, which can again form water. The production of $H_2CN$ upon impact between N and $CH_3$ radicals is prohibited due to competition with other reactions that consume $CH_3$ radicals upon the addition of $O_2$. As a result, the concentration of HCN in the mixture is greatly reduced.

The most important products in a 10:10:78:2 $CO_2/CH_4/N_2/O_2$ mixture, as predicted by our model, are (in order of decreasing importance) $H_2O$, CO, $H_2$, ethane ($C_2H_6$), methanol ($CH_3OH$), and hydrogen cyanide (HCN), with molar fractions of 1.60, 1.30, 0.78, 0.13, 0.10, and 0.094%, respectively. Note that methanol ($CH_3OH$) was not detected in our experiments because its concentration approaches the detection limit. In contrast, $C_3H_8$ species were detected despite their lower concentration because of a much lower detection limit.

The comparison of Figures 17 and 18 clearly shows that $O_2$ addition has a dramatic effect on the plasma chemistry of $CO_2$ and $CH_4$ conversion, as was also clear from Section 3.2 and Sections 3.3.1−3.3.6 (cf. Figure 9 and Figures S2, S5, S8, S11, S14, and S17 of the SI). A similar behavior was reported by De Bie et al. when comparing the plasma chemistry of DRM ($CH_4/CO_2$) and POX ($CH_4/O_2$). Indeed, both investigations indicate that mixtures with $CO_2$ favor the formation of $H_2$, while the production of $H_2O$ is greatly promoted upon the addition of $O_2$. CO is formed at high density in both gas mixtures. Note that adding $O_2$ can effectively promote the conversion of $CH_4$ (see Figure 9). However, also a significant amount of undesired $CO_2$ is formed and thus the net conversion of $CO_2$ is greatly reduced. Our pathway analysis shows how plasma chemistry modeling can help to obtain better insight, and this is very valuable to optimize the process. For example, the different pathways revealed by our model can help to determine the most suitable feed gas ratio to obtain the highest yield or selectivity of desired products.

## 4. CONCLUSIONS AND OUTLOOK

Chemical kinetics modeling has proven to be very useful to study the plasma-based conversion of $CO_2$ and $CH_4$. In recent years, plasma chemistry models have been developed in a stepwise manner. First models consisted of single-component molecular gases, that is, to study $CO_2$ splitting and $CH_4$ reforming. In a next step, multicomponent mixtures were studied, that is, DRM, POX, artificial photosynthesis, and $CO_2$ hydrogenation. Subsequently, the effect of $N_2$ as impurity and admixture on the $CO_2$ splitting and $CH_4$ reforming process was investigated to better approach real effluent gases.

Combining the knowledge gathered in this field so far, we presented here a new comprehensive plasma chemistry set that can be used for zero-dimensional modeling of the chemical kinetics in low-temperature plasmas for all possible combinations of $CO_2$, $CH_4$, $N_2$, $O_2$, and $H_2O$ for a wide variety of applications. It will be useful, for instance, for $CO_2$ conversion studies in the presence of both $CH_4$ and $N_2$ as well as for unravelling the possibilities of plasma-based multireforming processes. Furthermore, also in other fields, such as (plasma-assisted) combustion and even more exotic applications, like planetary atmosphere and spacecraft re-entry modeling, this chemistry set could also be used as a foundation to build a comprehensive computational data set.

This comprehensive model was first validated by comparing the calculated $CO_2$ (and $CH_4$) conversion for pure $CO_2$ as well as $CO_2/CH_4$, $CO_2/N_2$, $CH_4/N_2$, and $CO_2/H_2O$ gas mixtures, with experimental data from our previous work. Subsequently, a more extensive validation was performed by a combined calculation and experimental study, investigating the conversion of $CH_4$ and $CO_2$ as well as the selectivity of the major products in a $CO_2/CH_4/N_2$ mixture for varying $CO_2/CH_4$ ratios and $N_2$ contents as well as upon $O_2$ and $H_2O$ addition. Good agreement was reached with the experimental data, indicating that the chemical kinetics model sufficiently captures the underlying plasma chemistry for these processes.

The presence of $N_2$ in a $CO_2/CH_4$ gas mixture clearly enhances the absolute $CO_2$ and $CH_4$ conversion due to dissociation of $CO_2$ and $CH_4$ upon collision with nitrogen metastable molecules (mainly $N_2(a'\Sigma_u^-)$ and $N_2(a'\Sigma_u^-)$), and it also yields a slight increase in the syngas ($H_2/CO$) ratio. This is because the $N_2$ metastable molecules contribute more to the dissociation of $CH_4$, yielding $H_2$, due to the higher dissociation rate than that of $CO_2$. Moreover, at a fixed $CH_4$ content of 10%, increasing the $CO_2/CH_4$ mixing ratio from 0.5 to 4, by modifying the $N_2$ content, yields a drop in the $H_2/CO$ ratio from 2.45 to 0.42. These results show that we can exert great control over the $H_2/CO$ ratio by changing the mixing ratio.

Although the addition of $O_2$ is also beneficial for the $CH_4$ conversion, due to a shift toward POX over DRM, it is accompanied by a severe drop in $CO_2$ conversion and syngas ratio. Furthermore, a large fraction of the converted $CH_4$ is transformed into $H_2O$ rather than value-added products.

The addition of $H_2O$ had virtually no effect on the $CH_4$ and $CO_2$ conversion. This is interesting because in a pure $CO_2/H_2O$ mixture $H_2O$ addition leads to a drop in $CO_2$ conversion.[73] The reason is that the H atoms, originating from $CH_4$ dissociation, react with the OH radicals, so that the latter do not recombine with CO into $CO_2$, which is the limiting process in the $CO_2/H_2O$ mixture.[73] Additionally, the syngas ratio increases due to the effective conversion of $H_2O$ into $H_2$.

Although this new chemical kinetics model already yields good agreement with experimental data for various gas mixtures and a wide range of mixing ratios, we should remain cautious when using its results; this is true for any model. The chemistry set contains 1729 reactions, each with its corresponding cross section or rate coefficient, which are subject to certain uncertainties.[94] The latter will, of course, be reflected in the results. A crucial next step in the field of plasma chemistry modeling should consist of performing a detailed uncertainty analysis and sensitivity studies. By doing so, the impact of these uncertainties on the model predictions can be revealed, and the accuracy of the model can be determined. Such an analysis was presented already for less complicated mixtures, that is, by Turner for a $He/O_2$ mixture[95−97] and in our group for a $CO_2$ plasma.[38] Although this will be a huge amount of work, we will continue along these lines because it is indispensable to fully explore the predictive character of such a model.

Additionally, the model presented here mainly applies to a DBD plasma reactor, which has been mostly used for gas conversion studies up to now. However, other types of plasmas are also gaining increasing interest, like microwave plasmas and gliding arc discharges.[11] They operate under somewhat different conditions, such as lower reduced electric field (i.e., ratio of electric field over gas density) around 50−100 Td. Under these conditions, the electron temperature is on the order of 1 eV, which is most suitable for vibrational excitation. The low vibrational levels



DOI: 10.1021/acs.jpcc.7b10619
J. Phys. Chem. C 2018, 122, 8704−8723

will gradually populate higher vibrational levels by vibration−vibration collisions (so-called VV relaxation), and the highest vibrational levels will easily dissociate. Hence, this process of vibrational ladder climbing leading to dissociation is the most energy-efficient process for $CO_2$ dissociation. This explains why $CO_2$ dissociation is quite energy efficient in microwave and gliding arc discharges.[4,11] These processes are not considered in detail in the model presented here because they are of minor importance in a DBD. However, a detailed model for the $CO_2$ vibrational kinetics has already been developed within the group PLASMANT[34,35] as well as models for $CO_2/N_2$ and $N_2/O_2$ mixtures, accounting in detail for the vibrational kinetics of $CO_2$, $N_2$, and $O_2$.[6,82] In the future, it would be useful to extend this newly developed model for the $CO_2/CH_4/N_2/O_2/H_2O$ mixture with the vibrational kinetics of the various molecules so that this model becomes applicable to other plasma types as well. Not only is this true for the $CO_2$ vibrational levels, but also the $N_2$ vibrational levels can be important for $CO_2$ (and maybe $CH_4$) dissociation.[82] Furthermore, when the $CO_2$ conversion is significant, the CO vibrational kinetics should be considered as well, in relation to the formation of C and O atoms.[98] Again, adding the vibrational levels of all of these molecules will require major efforts, in view of the possible coupling between all these vibrational levels, and keeping in mind uncertainties in all rate coefficients[95−97] and the approximations that need to be made.[15,16]

This combined computational and experimental study reveals that the major products formed by mixtures of $CO_2$, $CH_4$, $N_2$, $O_2$, and $H_2O$ are syngas and some higher hydrocarbons (mainly $C_2H_6$ and $C_3H_8$) as well as $H_2O$, while the concentrations of oxygenates like methanol, formic acid, formaldehyde, as well as hydrogen cyanide are almost negligible. Hence, to increase the product selectivity of future plasma-based reforming processes, preferably to these oxygenates, combinations with a catalyst or membranes will be necessary. This brings us to another future necessity in the field of plasma chemistry modeling, that is, the need to extend these models with surface reactions, as recently done for $NH_3$ synthesis by Hong et al.[99] This step would make it possible for 0D plasma chemistry models to account for plasma catalysis and thus to make it possible to predict the requirements of the underlying plasmachemical pathways to selectively produce the desired value-added compounds. This stresses the power that lies within this type of modeling studies, that is, to unravel the underlying chemical pathways to obtain a better understanding of the chemistry taking place, which, in turn, allows us to predict whether new conditions could be more promising and help to point experiments in the right direction.

## ■ ASSOCIATED CONTENT

### Supporting Information

The Supporting Information is available free of charge on the ACS Publications website at DOI: 10.1021/acs.jpcc.7b10619.

Overview of the reactions included in the model (PDF)

## ■ AUTHOR INFORMATION


### Corresponding Authors

*W.W.: E-mail: wangweizong@gmail.com.
*R.S.: E-mail: ramses.snoeckx@uantwerpen.be.
*A.B.: E-mail: annemie.bogaerts@uantwerpen.be.

### ORCID

Ramses Snoeckx: 0000-0002-3911-4035
Xuming Zhang: 0000-0003-4665-7641
Annemie Bogaerts: 0000-0001-9875-6460

### Author Contributions

‖W.W. and R.S. contributed equally to this work.


### Notes

The authors declare no competing financial interest.

### Biographies

Photo provided by Quanzhi Zhang.

Weizong Wang was born in Shandong, China in 1984. He received double Ph.D. degrees in electrical engineering from Xi'an Jiaotong University, China and University of Liverpool, United Kingdom in 2013. Since then, he worked at Qian Xuesen Laboratory of Space Technology in China until 2015, focusing on plasma propulsion. Currently, he is working in the PLASMANT research group at the University of Antwerp in Belgium supported by the Marie Skłodowska-Curie Individual Fellowship towards a better understanding of plasma-based gas conversion into value-added products. His main interests concern the fundamental physics, chemistry, and applications of low-temperature plasmas.

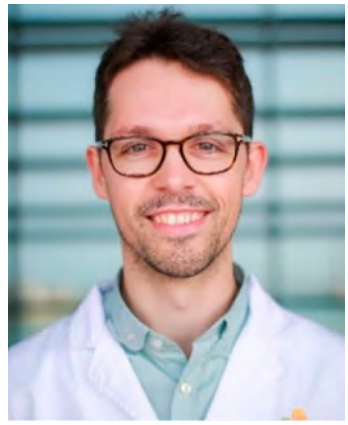

Photo provided by Louisa Belanger.

Ramses Snoeckx, born in 1988, obtained Master's degrees in both environmental science and chemistry. Combining these specializations, he successfully obtained a Ph.D. in chemistry (2017, University of Antwerp) for his research on plasma-based conversion of greenhouse gases into value-added chemicals and fuels. Currently, he is working as a postdoctoral fellow at the King Abdullah University of Science and Technology (KAUST). The underlying chemical reactions taking place in plasmas are his prime focus. By relying on a combination of modelling and experimental techniques, he aims to gain the necessary insights into the plasmachemical pathways to improve existing—as well as to find new—applications for plasma-based environmental and energy solutions.



DOI: 10.1021/acs.jpcc.7b10619
J. Phys. Chem. C 2018, 122, 8704−8723

Photo provided by Jingyi Han.

Xuming Zhang was born in Hangzhou, China in 1981. He received Ph.D. degree from Zhejiang University, China in 2011. He served King Abdullah University of Science and Technology (KAUST) as a postdoctoral research fellow from 2011 to 2015. He has been with Zhejiang Gongshang University as an assistant professor since 2016. Dr. Zhang has authored over 30 publications in peer-reviewed journals. His current research interests include nonthermal plasma generation and plasma-induced fuel reforming and environmental remediation.

Photo provided by Thibault Guiberti.

Min Suk Cha was born in Seoul, Korea in 1970. He received Ph. D. degrees in mechanical engineering from Seoul National University in 1999, specializing in Combustion Science. He worked at the Korea Institute of Machinery & Materials (KIMM), where he obtained a plasma background, as a Principal Research Scientist from 2000 to 2010. Currently, he is associate professor at King Abdullah University of Science and Technology (KAUST). His current research interests include plasma (and electrically) assisted combustion, plasma fuel reforming, and in-liquid plasma generations.

Photo provided by Wim Schelles.

Annemie Bogaerts, born in 1971, obtained her Ph.D. in chemistry in 1996 from the University of Antwerp in Belgium. She became professor of physical chemistry in 2003 at this university and has been a full professor since 2012. She is head of the interdisciplinary research group PLASMANT. The research activities of her group include modelling of plasma chemistry, plasma reactor design, and plasma–surface interactions as well as plasma experiments for various applications, including environmental and medical applications (mainly cancer treatment) as well as nanotechnology and analytical chemistry. In recent years, special attention has been given to $CO_2$ conversion by plasma and plasma catalysis.

## ■ ACKNOWLEDGMENTS

We acknowledge financial support from the European Marie Skłodowska-Curie Individual Fellowship "GlidArc" within Horizon2020 (Grant No. 657304), the Fund for Scientific Research Flanders (FWO) (grant nos G.0217.14N, G.0254.14N, and G.0383.16N), Competitive Research1 Funding from King Abdullah University of Science and Technology (KAUST), the IAP/7 (Interuniversity Attraction Pole) program 'PSI-Physical Chemistry of Plasma-Surface Interactions', financially supported by the Belgian Federal Office for Science Policy (BELSPO), as well as the Fund for Scientific Research Flanders (FWO). This work was carried out in part using the Turing HPC infrastructure at the CalcUA core facility of the Universiteit Antwerpen, a division of the Flemish Supercomputer Center VSC, funded by the Hercules Foundation, the Flemish Government (department EWI), and the University of Antwerp.

## ■ REFERENCES

(1) Adamovich, I.; Baalrud, S. D.; Bogaerts, A.; Bruggeman, P. J.; Cappelli, M.; Colombo, V.; Czarnetzki, U.; Ebert, U.; Eden, J. G.; Favia, P.; et al. The 2017 Plasma Roadmap: Low Temperature Plasma Science and Technology. *J. Phys. D: Appl. Phys.* **2017**, *50*, 323001.

(2) Lee, C. G. N.; Kanarik, K. J.; Gottscho, R. A. The Grand Challenges of Plasma Etching: A Manufacturing Perspective. *J. Phys. D: Appl. Phys.* **2014**, *47*, 273001.

(3) Bogaerts, A.; Neyts, E.; Gijbels, R.; van der Mullen, J. Gas Discharge Plasmas and Their Applications. *Spectrochim. Acta, Part B* **2002**, *57*, 609–658.

(4) Fridman, A. *Plasma Chemistry*; Cambridge University Press: New York, 2008.

(5) Chang, J. S. Recent Development of Plasma Pollution Control Technology: A Critical Review. *Sci. Technol. Adv. Mater.* **2001**, *2*, 571–576.

(6) Wang, W.; Patil, B.; Heijkers, S.; Hessel, V.; Bogaerts, A. Nitrogen Fixation by Gliding Arc Plasma: Better Insight by Chemical Kinetics Modelling. *ChemSusChem* **2017**, *10*, 2145–2157.

(7) Patil, B. S.; Cherkasov, N.; Lang, J.; Ibhadon, A. O.; Hessel, V.; Wang, Q. Low Temperature Plasma-Catalytic NOx Synthesis in a Packed DBD Reactor: Effect of Support Materials and Supported Active Metal Oxides. *Appl. Catal., B* **2016**, *194*, 123–133.

(8) Chen, H. L.; Lee, H. M.; Chen, S. H.; Chao, Y.; Chang, M. B. Review of Plasma Catalysis on Hydrocarbon Reforming for Hydrogen Production—Interaction, Integration, and Prospects. *Appl. Catal., B* **2008**, *85*, 1–9.

(9) Snoeckx, R.; Rabinovich, A.; Dobrynin, D.; Bogaerts, A.; Fridman, A. Plasma Based Liquefaction of Methane: the Road from Hydrogen Production to Direct Methane Liquefaction. *Plasma Processes Polym.* **2017**, *14*, 1600115.

(10) Tu, X.; Whitehead, J. C. Plasma-Catalytic Dry Reforming of Methane in an Atmospheric Dielectric Barrier Discharge: Understanding the Synergistic Effect at Low Temperature. *Appl. Catal., B* **2012**, *125*, 439–448.

(11) Snoeckx, R.; Bogaerts, A. Plasma Technology – a Novel Solution for $CO_2$ Conversion? *Chem. Soc. Rev.* **2017**, *46*, 5805–5863.



DOI: 10.1021/acs.jpcc.7b10619
*J. Phys. Chem. C* 2018, 122, 8704–8723

(12) Neyts, E. C.; Bogaerts, A. Understanding Plasma Catalysis Through Modelling and Simulation—A Review. *J. Phys. D: Appl. Phys.* **2014**, *47*, 224010.
(13) Neyts, E. C.; Ostrikov, K.; Sunkara, M. K.; Bogaerts, A. Plasma Catalysis: Synergistic Effects at the Nanoscale. *Chem. Rev.* **2015**, *115*, 13408−13446.
(14) Whitehead, J. C. Plasma−catalysis: The Known Knowns, the Known Unknowns and the Unknown Unknowns. *J. Phys. D: Appl. Phys.* **2016**, *49*, 243001.
(15) Bogaerts, A.; De Bie, C.; Snoeckx, R.; Kozák, T. Plasma Based $CO_2$ and $CH_4$ Conversion: A Modeling Perspective. *Plasma Processes Polym.* **2017**, *14*, 1600070.
(16) Bogaerts, A.; Berthelot, A.; Heijkers, S.; Kolev, S.; Snoeckx, R.; Sun, S. R.; Trenchev, G.; Van Laer, K.; Wang, W. $CO_2$ Conversion by Plasma Technology: Insights from Modeling the Plasma Chemistry and Plasma Reactor Design. *Plasma Sources Sci. Technol.* **2017**, *26*, 063001.
(17) Zou, J. J.; Zhang, Y. P.; Liu, C. J.; Li, Y.; Eliasson, B. Starch-enhanced Synthesis of Oxygenates from Methane and Carbon Dioxide Using Dielectric-Barrier Discharges. *Plasma Chem. Plasma Process.* **2003**, *23*, 69−82.
(18) Kraus, M.; Eliasson, B.; Kogelschatz, U.; Wokaun, A. $CO_2$ Reforming of Methane by the Combination of Dielectric-Barrier Discharges and Catalysis. *Phys. Chem. Chem. Phys.* **2001**, *3*, 294−300.
(19) Mei, D. H.; Zhu, X. B.; He, Y. L.; Yan, J. D.; Tu, X. Plasma-assisted Conversion of $CO_2$ in A Dielectric Barrier Discharge Reactor: Understanding the Effect of Packing Materials. *Plasma Sources Sci. Technol.* **2015**, *24*, 015011.
(20) Tu, X.; Gallon, H. J.; Twigg, M. V.; Gorry, P. A.; Whitehead, J. C. Dry Reforming of Methane Over a $NI/AL_2O_3$ Catalyst in a Coaxial Dielectric Barrier Discharge Reactor. *J. Phys. D: Appl. Phys.* **2011**, *44*, 274007.
(21) IPCC. *Summary for Policymakers*, 2014.
(22) McDonough, W.; Braungart, M.; Anastas, P. T.; Zimmerman, J. B. Peer Reviewed: Applying the Principles of Green Engineering to Cradle-to-Cradle Design. *Environ. Sci. Technol.* **2003**, *37*, 434A−441A.
(23) Jiang, Z.; Xiao, T.; Kuznetsov, V. L.; Edwards, P. P. Turning Carbon Dioxide into Fuel. *Philos. Trans. R. Soc., A* **2010**, *368*, 3343−3364.
(24) Mikkelsen, M.; Jørgensen, M.; Krebs, F. C. The Teraton Challenge. A Review of Fixation and Transformation of Carbon Dioxide. *Energy Environ. Sci.* **2010**, *3*, 43−81.
(25) Ju, Y.; Sun, W. T. Plasma Assisted Combustion: Dynamics and Chemistry. *Prog. Energy Combust. Sci.* **2015**, *48*, 21−83.
(26) Starikovskaia, S. M. Plasma-assisted Ignition and Combustion: Nanosecond Discharges and Development of Kinetic Mechanisms. *J. Phys. D: Appl. Phys.* **2014**, *47*, 353001.
(27) Gokcen, T. $N_2$-$CH_4$-Ar Chemical Kinetic Model for Simulations of Atmospheric Entry to Titan. *J. Thermophys. Heat Transfer* **2007**, *21*, 9−18.
(28) Bultel, A.; Annaloro, J. Elaboration of Collisional−Radiative Models for Flows Related to Planetary Entries into the Earth and Mars Atmospheres. *Plasma Sources Sci. Technol.* **2013**, *22*, 025008.
(29) Aerts, R.; Somers, W.; Bogaerts, A. Carbon Dioxide Splitting in a Dielectric Barrier Discharge Plasma: A Combined Experimental and Computational Study. *ChemSusChem* **2015**, *8*, 702−716.
(30) Wang, W.; Berthelot, A.; Kolev, S.; Tu, X.; Bogaerts, A. $CO_2$ Conversion in a Gliding Arc Plasma: 1D Cylindrical Discharge Model. *Plasma Sources Sci. Technol.* **2016**, *25*, 065012.
(31) Wang, W.; Mei, D.; Tu, X.; Bogaerts, A. Gliding Arc Plasma for $CO_2$ Conversion: Better Insights by a Combined Experimental and Modelling Approach. *Chem. Eng. J.* **2017**, *330*, 11−25.
(32) Sun, S. R.; Wang, H. X.; Mei, D. H.; Tu, X.; Bogaerts, A. $CO_2$ Conversion in a Gliding Arc Plasma: Performance Improvement Based on Chemical Reaction Modeling. *J. $CO_2$ Util.* **2017**, *17*, 220−234.
(33) Aerts, R.; Martens, T.; Bogaerts, A. Influence of Vibrational States on $CO_2$ Splitting by Dielectric Barrier Discharges. *J. Phys. Chem. C* **2012**, *116*, 23257−23273.
(34) Kozák, T.; Bogaerts, A. Evaluation of the Energy Efficiency of $CO_2$ Conversion in Microwave Discharges Using a Reaction Kinetics Model. *Plasma Sources Sci. Technol.* **2015**, *24*, 015024.
(35) Kozák, T.; Bogaerts, A. Splitting of $CO_2$ by Vibrational Excitation in Non-Equilibrium Plasmas: A Reaction Kinetics Model. *Plasma Sources Sci. Technol.* **2014**, *23*, 045004.
(36) Berthelot, A.; Bogaerts, A. Modeling of Plasma-Based $CO_2$ Conversion: Lumping of the Vibrational Levels. *Plasma Sources Sci. Technol.* **2016**, *25*, 045022.
(37) Berthelot, A.; Bogaerts, A. Modeling of $CO_2$ Splitting in a Microwave Plasma: How to Improve the Conversion and Energy Efficiency. *J. Phys. Chem. C* **2017**, *121*, 8236−8251.
(38) Berthelot, A.; Bogaerts, A. Modeling of $CO_2$ Plasma: Effect of Uncertainties in the Plasma Chemistry. *Plasma Sources Sci. Technol.* **2017**, *26*, 115002.
(39) Koelman, P.; Heijkers, S.; Tadayon Mousavi, S.; Graef, W.; Mihailova, D.; Kozak, T.; Bogaerts, A.; van Dijk, J. A Comprehensive Chemical Model for the Splitting of $CO_2$ in Non-Equilibrium Plasmas. *Plasma Processes Polym.* **2017**, *14*, 1−20.
(40) Ponduri, S.; Becker, M. M.; Welzel, S.; Van De Sanden, M. C. M.; Loffhagen, D.; Engeln, R. Fluid Modelling of $CO_2$ Dissociation in a Dielectric Barrier Discharge. *J. Appl. Phys.* **2016**, *119*, 093301.
(41) Pietanza, L. D.; Colonna, G.; D'Ammando, G.; Laricchiuta, A.; Capitelli, M. Non Equilibrium Vibrational Assisted Dissociation and Ionization Mechanisms in Cold $CO_2$ Plasmas. *Chem. Phys.* **2016**, *468*, 44−52.
(42) Pietanza, L. D.; Colonna, G.; D'Ammando, G.; Laricchiuta, A.; Capitelli, M. Electron Energy Distribution Functions and Fractional Power Transfer In "cold" and Excited $CO_2$ Discharge and Post Discharge Conditions. *Phys. Plasmas* **2016**, *23*, 013515.
(43) Pietanza, L. D.; Colonna, G.; Laporta, V.; Celiberto, R.; D'Ammando, G.; Laricchiuta, A.; Capitelli, M. Influence of Electron Molecule Resonant Vibrational Collisions over the Symmetric Mode and Direct Excitation-Dissociation Cross Sections of $CO_2$ on the Electron Energy Distribution Function and Dissociation Mechanisms in Cold Pure $CO_2$ Plasmas. *J. Phys. Chem. A* **2016**, *120*, 2614−2628.
(44) Pietanza, L. D.; Colonna, G.; D'Ammando, G.; Capitelli, M. Time-Dependent Coupling of Electron Energy Distribution Function, Vibrational Kinetics of the Asymmetric Mode of $CO_2$ and Dissociation, Ionization and Electronic Excitation Kinetics under Discharge and Post-Discharge Conditions. *Plasma Phys. Controlled Fusion* **2017**, *59*, 014035.
(45) Pietanza, L. D.; Colonna, G.; D'Ammando, G.; Laricchiuta, a; Capitelli, M. Vibrational Excitation and Dissociation Mechanisms of $CO_2$ under Non-Equilibrium Discharge and Post-Discharge Conditions. *Plasma Sources Sci. Technol.* **2015**, *24*, 042002.
(46) Capitelli, M.; Colonna, G.; D'Ammando, G.; Hassouni, K.; Laricchiuta, A.; Pietanza, L. D. Coupling of Plasma Chemistry, Vibrational Kinetics, Collisional-Radiative Models and Electron Energy Distribution Function Under Non-Equilibrium Conditions. *Plasma Processes Polym.* **2017**, *14*, 1600109.
(47) Moss, M. S.; Yanallah, K.; Allen, R. W. K.; Pontiga, F. An Investigation of $CO_2$ Splitting Using Nanosecond Pulsed Corona Discharge: Effect of Argon Addition on $CO_2$ Conversion and Energy Efficiency. *Plasma Sources Sci. Technol.* **2017**, *26*, 035009.
(48) Cheng, J.-L.; Wang, H.-X.; Sun, S.-R. Analysis of Dissociation Mechanism of $CO_2$ in a Micro-Hollow Cathode Discharge. *Chin. Phys. Lett.* **2016**, *33*, 108201.
(49) de la Fuente, J. F.; Moreno, S. H.; Stankiewicz, A. I.; Stefanidis, G. D. A New Methodology for the Reduction of Vibrational Kinetics in Non-Equilibrium Microwave Plasma: Application to $CO_2$ Dissociation. *React. Chem. Eng.* **2016**, *1*, 540−554.
(50) Indarto, A.; Choi, J.; Lee, H.; Song, H. K. Kinetic Modeling of Plasma Methane Conversion Using Gliding Arc. *Plasma Devices Oper.* **2005**, *14*, 13−21.
(51) Indarto, A.; Coowanitwong, N.; Choi, J. W.; Lee, H.; Song, H. K. Kinetic Modeling of Plasma Methane Conversion in a Dielectric Barrier Discharge. *Fuel Process. Technol.* **2008**, *89*, 214−219.
(52) De Bie, C.; Verheyde, B.; Martens, T.; van Dijk, J.; Paulussen, S.; Bogaerts, A. Fluid Modeling of the Conversion of Methane into Higher


DOI: 10.1021/acs.jpcc.7b10619
J. Phys. Chem. C 2018, 122, 8704−8723

Hydrocarbons in an Atmospheric Pressure Dielectric Barrier Discharge. *Plasma Processes Polym.* **2011**, *8*, 1033−1058.
(53) Yang, Y. Direct Non-Oxidative Methane Conversion by Non-Thermal Plasma: Modeling Study. *Plasma Chem. Plasma Process.* **2003**, *23*, 327−346.
(54) Luche, J.; Aubry, O.; Khacef, A.; Cormier, J.-M. Syngas Production from Methane Oxidation Using a Non-Thermal Plasma: Experiments and Kinetic Modeling. *Chem. Eng. J.* **2009**, *149*, 35−41.
(55) Zhou, L. M.; Xue, B.; Kogelschatz, U.; Eliasson, B. Non-equilibrium Plasma Reforming of Greenhouse Gases to Synthesis Gas. *Energy Fuels* **1998**, *12*, 1191−1199.
(56) Machrafi, H.; Cavadias, S.; Amouroux, J. Valorization by Means of Dielectric Barrier Discharge. *J. Phys. Conf. Ser.* **2011**, *275*, 012016.
(57) Goujard, V.; Tatibouët, J. M.; Batiot-Dupeyrat, C. Carbon Dioxide Reforming of Methane Using a Dielectric Barrier Discharge Reactor: Effect of Helium Dilution and Kinetic Model. *Plasma Chem. Plasma Process.* **2011**, *31*, 315−325.
(58) Wang, J. G.; Liu, C. J.; Eliassion, B. Density Functional Theory Study of Synthesis of Oxygenates and Higher Hydrocarbons from Methane and Carbon Dioxide Using Cold Plasmas. *Energy Fuels* **2004**, *18*, 148−153.
(59) Istadi, I.; Amin, N. A. S. Modelling and Optimization of Catalytic-Dielectric Barrier Discharge Plasma Reactor for Methane and Carbon Dioxide Conversion Using Hybrid Artificial Neural Network-Genetic Algorithm Technique. *Chem. Eng. Sci.* **2007**, *62*, 6568−6581.
(60) Kraus, M.; Egli, W.; Haffner, K.; Eliasson, B.; Kogelschatz, U.; Wokaun, A. Investigation of Mechanistic Aspects of the Catalytic $CO_2$ Reforming of Methane in a Dielectric-Barrier Discharge Using Optical Emission Spectroscopy and Kinetic Modeling. *Phys. Chem. Chem. Phys.* **2002**, *4*, 668−675.
(61) Liu, C.-J.; Li, Y.; Zhang, Y.-P.; Wang, Y.; Zou, J.; Eliasson, B.; Xue, B. Production of Acetic Acid Directly from Methane and Carbon Dioxide Using Dielectric-Barrier Discharges. *Chem. Lett.* **2001**, *30*, 1304−1305.
(62) Janeco, A.; Pinhao, N. R.; Guerra, V. Electron Kinetics in He/$CH_4$/$CO_2$ Mixtures Used for Methane Conversion. *J. Phys. Chem. C* **2015**, *119*, 109.
(63) Snoeckx, R.; Aerts, R.; Tu, X.; Bogaerts, A. Plasma-Based Dry Reforming: A Computational Study Ranging from the Nanoseconds to Seconds Time Scale. *J. Phys. Chem. C* **2013**, *117*, 4957−4970.
(64) Snoeckx, R.; Zeng, Y. X.; Tu, X.; Bogaerts, A. Plasma-Based Dry Reforming: Improving the Conversion and Energy Efficiency in a Dielectric Barrier Discharge. *RSC Adv.* **2015**, *5*, 29799−29808.
(65) De Bie, C.; Martens, T.; van Dijk, J.; Paulussen, S.; Verheyde, B.; Corthals, S.; Bogaerts, A. Dielectric Barrier Discharges Used for the Conversion of Greenhouse Gases: Modeling the Plasma Chemistry by Fluid Simulations. *Plasma Sources Sci. Technol.* **2011**, *20*, 024008.
(66) De Bie, C.; Van Dijk, J.; Bogaerts, A. The Dominant Pathways for the Conversion of Methane into Oxygenates and Syngas in an Atmospheric Pressure Dielectric Barrier Discharge. *J. Phys. Chem. C* **2015**, *119*, 22331−22350.
(67) Zhou, L. M.; Xue, B.; Kogelschatz, U.; Eliasson, B. Partial Oxidation of Methane to Methanol with Oxygen or Air in a Nonequilibrium Discharge Plasma. *Plasma Chem. Plasma Process.* **1998**, *18*, 375−393.
(68) Nair, S. A.; Nozaki, T.; Okazaki, K. Methane Oxidative Conversion Pathways in a Dielectric Barrier Discharge Reactor-Investigation of Gas Phase Mechanism. *Chem. Eng. J.* **2007**, *132*, 85−95.
(69) Goujard, V.; Nozaki, T.; Yuzawa, S.; Ağiral, A.; Okazaki, K. Plasma-Assisted Partial Oxidation of Methane at Low Temperatures: Numerical Analysis of Gas-Phase Chemical Mechanism. *J. Phys. D: Appl. Phys.* **2011**, *44*, 274011.
(70) Nozaki, T.; Aĝiral, A.; Yuzawa, S.; Han Gardeniers, J. G. E.; Okazaki, K. A Single Step Methane Conversion Into Synthetic Fuels Using Microplasma Reactor. *Chem. Eng. J.* **2011**, *166*, 288−293.
(71) Zhou, J.; Xu, Y.; Zhou, X.; Gong, J.; Yin, Y.; Zheng, H.; Guo, H. Direct Oxidation of Methane to Hydrogen Peroxide and Organic Oxygenates in a Double Dielectric Plasma Reactor. *ChemSusChem* **2011**, *4*, 1095−1098.
(72) Matin, N. S.; Whitehead, J. C. A Chemical Model for the Atmospheric Pressure Plasma Reforming of Methane with Oxygen. *28th ICPIG* **2007**, 983−986.
(73) Snoeckx, R.; Ozkan, A.; Reniers, F.; Bogaerts, A. The Quest for Value-Added Products from Carbon Dioxide and Water in a Dielectric Barrier Discharge: A Chemical Kinetics Study. *ChemSusChem* **2017**, *10*, 409−424.
(74) De Bie, C.; Van Dijk, J.; Bogaerts, A. $CO_2$ Hydrogenation in a Dielectric Barrier Discharge Plasma Revealed. *J. Phys. Chem. C* **2016**, *120*, 25210−25224.
(75) Ding, K.; Lieberman. Reaction Pathways for Bio-Active Species in a He/$H_2O$ Atmospheric Pressure Capacitive Discharge. *J. Phys. D: Appl. Phys.* **2015**, *48*, 035401.
(76) Legrand, J. C.; Diamy, A. M.; Hrach, R.; Hrachova, V. Kinetics of Reactions in $CH_4$/$N_2$ Afterglow Plasma. *Vacuum* **1997**, *48*, 671−675.
(77) Majumdar, A.; Behnke, J. F.; Hippler, R.; Matyash, K.; Schneider, R. Chemical Reaction Studies in $CH_4$/Ar and $CH_4$/$N_2$ Gas Mixtures of a Dielectric Barrier Discharge. *J. Phys. Chem. A* **2005**, *109*, 9371−9377.
(78) Pintassilgo, C. D.; Jaoul, C.; Loureiro, J.; Belmonte, T.; Czerwiec, T. Kinetic Modelling of a $N_2$ Flowing Microwave Discharge with $CH_4$ Addition in the Post-Discharge for Nitrocarburizing Treatments. *J. Phys. D: Appl. Phys.* **2007**, *40*, 3620−3632.
(79) Jauberteau, J. L.; Jauberteau, I.; Cinelli, M. J.; Aubreton, J. Reactivity of Methane in a Nitrogen Discharge Afterglow. *New J. Phys.* **2002**, *4*, 39.
(80) Savinov, S. Y.; Lee, H.; Song, H. K.; Na, B. K. The Effect of Vibrational Excitation of Molecules on Plasmachemical Reactions Involving Methane and Nitrogen. *Plasma Chem. Plasma Process.* **2003**, *23*, 159−173.
(81) Snoeckx, R.; Setareh, M.; Aerts, R.; Simon, P.; Maghari, A.; Bogaerts, A. Influence of $N_2$ Concentration in a $CH_4$/$N_2$ Dielectric Barrier Discharge Used for $CH_4$ Conversion into $H_2$. *Int. J. Hydrogen Energy* **2013**, *38*, 16098−16120.
(82) Heijkers, S.; Snoeckx, R.; Kozák, T.; Silva, T.; Godfroid, T.; Britun, N.; Snyders, R.; Bogaerts, A. $CO_2$ Conversion in a Microwave Plasma Reactor in the Presence of $N_2$: Elucidating the Role of Vibrational Levels. *J. Phys. Chem. C* **2015**, *119*, 12815−12828.
(83) Snoeckx, R.; Heijkers, S.; Van Wesenbeeck, K.; Lenaerts, S.; Bogaerts, A. $CO_2$ Conversion in a Dielectric Barrier Discharge Plasma: $N_2$ in the Mix as a Helping Hand or Problematic Impurity? *Energy Environ. Sci.* **2016**, *9*, 999−1011.
(84) Zhang, X.; Cha, M. S. Electron-Induced Dry Reforming of Methane in a Temperature-Controlled Dielectric Barrier Discharge Reactor. *J. Phys. D: Appl. Phys.* **2013**, *46*, 415205.
(85) Zhang, X.; Cha, M. S. Partial Oxidation of Methane in a Temperature-Controlled Dielectric Barrier Discharge Reactor. *Proc. Combust. Inst.* **2015**, *35*, 3447−3454.
(86) van Dijk, J.; Kroesen, G. M. W.; Bogaerts, A. Plasma Modeling and Numerical Simulation. *J. Phys. D: Appl. Phys.* **2009**, *42*, 190301.
(87) Bogaerts, A.; Alves, L. L. Special Issue on Numerical Modeling of Low-Temperature Plasmas for Various Applications − Part I: Review and Tutorial Papers on Numerical Modeling Approaches. *Plasma Processes Polym.* **2017**, *14*, 1690011.
(88) Alves, L. L.; Bogaerts, A.; Guerra, V.; Turner, M. M. Foundations of Modelling of Low-Temperature Plasmas. *Plasma Sources Sci. Technol.* **2018**, DOI: 10.1088/1361-6595/aaa86d.
(89) Van Gaens, W.; Bogaerts, A. Kinetic Modelling for an Atmospheric Pressure Argon Plasma Jet in Humid Air. *J. Phys. D: Appl. Phys.* **2013**, *46*, 275201.
(90) Zhou, L. M.; Xue, B.; Kogelschatz, U.; Eliasson, B. Non-equilibrium Plasma Reforming of Greenhouse Gases to Synthesis Gas. *Energy Fuels* **1998**, *12*, 1191−1199.
(91) Zhang, K.; Kogelschatz, U.; Eliasson, B. Conversion of Greenhouse Gases to Synthesis Gas and Higher Hydrocarbons. *Energy Fuels* **2001**, *15*, 395−402.
(92) Aerts, R.; Snoeckx, R.; Bogaerts, A. In-Situ Chemical Trapping of Oxygen in the Splitting of Carbon Dioxide by Plasma. *Plasma Processes Polym.* **2014**, *11*, 985−994.


DOI: 10.1021/acs.jpcc.7b10619
*J. Phys. Chem. C* 2018, 122, 8704−8723

(93) Atkins, P. W. *The Elements of Physical Chemistry*, 3rd ed.; Oxford University Press, 1993.
(94) Bogaerts, A.; Wang, W.; Berthelot, A.; Guerra, V. Modeling Plasma-based $CO_2$ Conversion: Crucial Role of the Dissociation Cross Section. *Plasma Sources Sci. Technol.* **2016**, *25*, 055016.
(95) Turner, M. M. Uncertainty and Error in Complex Plasma Chemistry Models. *Plasma Sources Sci. Technol.* **2015**, *24*, 035027.
(96) Turner, M. M. Uncertainty and Sensitivity Analysis in Complex Plasma Chemistry Models. *Plasma Sources Sci. Technol.* **2016**, *25*, 015003.
(97) Turner, M. M. Computer Simulation in Low-Temperature Plasma Physics: Future Challenges. *Plasma Processes Polym.* **2017**, *14*, 1600121.
(98) Pietanza, L. D.; Colonna, G.; Capitelli, M. Non-equilibrium Plasma Kinetics of Reacting CO: An Improved State to State Approach. *Plasma Sources Sci. Technol.* **2017**, *26*, 125007.
(99) Hong, J.; Pancheshnyi, S.; Tam, E.; Lowke, J. J.; Prawer, S.; Murphy, A. B. Kinetic Modelling of $NH_3$ Production in $N_2$–$H_2$ Non-Equilibrium Atmospheric-Pressure Plasma Catalysis. *J. Phys. D: Appl. Phys.* **2017**, *50*, 154005.



DOI: 10.1021/acs.jpcc.7b10619
*J. Phys. Chem. C* 2018, 122, 8704–8723